



# The Effect of Chemisorption on the Chemical Evolution of Star-forming Regions

Kinsuk Acharyya<sup>1</sup> , Sean W. Schulte<sup>2</sup>, and Eric Herbst<sup>2,3</sup>

<sup>1</sup> Planetary Science Division, Physical Research Laboratory, Ahmedabad, 380009, India; [acharyya@prl.res.in](mailto:acharyya@prl.res.in)

<sup>2</sup> Department of Chemistry, University of Virginia, Charlottesville, VA 22904, USA

<sup>3</sup> Department of Astronomy, University of Virginia, Charlottesville, VA 22904, USA

Received 2019 September 25; revised 2019 December 13; accepted 2019 December 23; published 2020 February 20

## Abstract

We have studied the production of simple molecules on interstellar dust grains involving strong bonding via chemisorption on a graphite surface. Two classes of chemical simulations were run: models under isothermal conditions at temperatures from 150 to 400 K at 25 K intervals, and warm-up models starting at 10 K. For the isothermal models, physisorption does not occur appreciably, whereas for the warm-up models, it dominates at the lower temperatures before thermal desorption becomes rapid. We have made several simple approximations to determine what role, if any, chemisorption can play in the surface chemistry that occurs at temperatures above which icy mantles no longer cover the surface of dust grains. Our major finding is that the importance of chemisorption is greatly dependent on the efficiency of adsorption. Models having the lowest adsorption barrier show maximum abundances of chemisorbed species. Species such as CO, which are very efficiently formed in the gas phase at almost all temperatures (10–400 K), will not be strongly impacted by the existence of chemisorbed species. However, chemisorbed CO can achieve a reasonably high abundance ( $\sim 10^{-6}$ ). Species such as C<sub>2</sub>H<sub>2</sub> and NH<sub>3</sub>, which are less efficiently formed compared with CO in the gas phase, may show a change in their gas-phase abundance due to chemisorption. Several examples of this class of species can also show reasonably high abundances on grain surfaces due to chemisorption when the adsorption barrier is low.

*Unified Astronomy Thesaurus concepts:* [Astrochemistry \(75\)](#); [Interstellar medium \(847\)](#); [Interstellar molecules \(849\)](#); [Molecule formation \(2076\)](#); [Interstellar dust \(836\)](#)

## 1. Introduction

Molecular material can be found in a wide variety of astronomical conditions, ranging from low-temperature interstellar clouds to outer envelopes of carbon stars, and from objects in our own solar system to distant galaxies. An understanding of the formation of these molecules in diverse sources using numerical simulations has become an active topic of research. These molecules are synthesized both in the gas phase and on the surfaces of interstellar dust grains. The gas-phase processes in the simulations occur at temperatures from 10 to 800 K while reactions on dust surfaces normally occur at temperatures of up to 300 K. At higher grain temperatures, much of the ice mantle that had been formed desorbs into the gas, and the surfaces of dust grains become bare, as they had in earlier stages before the dense cloud stage. The bare dust grains are once again composed of silicates such as olivine and carbonaceous material. Despite the high temperatures, chemistry can occur on the bare dust grains following the formation of strong chemical bonds between adsorbates and the bare grains; the term for these bonds is chemisorption. Despite the fact that chemisorption can drive a high-temperature surface chemistry, very little attention has been paid to it in the astrochemical literature, to the best of our knowledge.

It was understood early in the history of astrochemistry that molecular hydrogen in the interstellar medium could only be produced efficiently via the recombination of two hydrogen atoms on grain surfaces. Nevertheless, the first sets of astrochemical models constructed to explain observed abundances in low-temperature dense interstellar clouds relied mainly on gas-phase ion–molecule reactions (Herbst & Klemperer 1973; Millar & Freeman 1984). Models that include chemistry on low-temperature grain surfaces for the formation of numerous species were introduced shortly

thereafter by Allen & Robinson (1977), Pickles & Williams (1977), and Tielens & Hagen (1982). Although different mechanisms were assumed by early authors, the idea developed that the dominant surface chemistry involved diffusion of surface species, the so-called Langmuir–Hinshelwood (LH) mechanism. The diffusion occurs by species bound loosely to the grains by weak electrostatic forces known as physisorption (Hasegawa et al. 1992). At a surface temperature of 10 K, only the lightest species, such as atomic and molecular hydrogen, can diffuse rapidly enough to cause surface reactions, but as the temperature increases, larger species begin to diffuse rapidly enough to react with one another when they collide as long as there is little chemical activation energy, or the energy barrier can be tunneled under. This constraint leads to the importance of radical–radical reactions in the surface chemistry, where such species can be formed from more stable ones by photodissociation with photons created by cosmic-ray bombardment (Garrod et al. 2008; Herbst & van Dishoeck 2009). Current simulations for diverse sources from low to high temperatures contain both surface chemistry and gas-phase chemistry. In addition to occurring via diffusion, the surface chemistry can occur via the Eley–Rideal (ER) mechanism, in which a gas-phase species lands atop a stationary adsorbate. A recent review, with an emphasis on complex molecules, has been given by Herbst (2017). Nevertheless, such networks do not include high-temperature surface chemistry, which must be governed by chemisorption because molecules attached to grains via weak forces do not reside long enough to react.

Although high-temperature chemistry has not been included on grains in general up to the present, its role has been studied in the formation of hydrogen. Cazaux & Tielens (2002) studied H<sub>2</sub> formation using both physisorbed

and chemisorbed sites on grain surfaces, and found that  $H_2$  formation is efficient up to a dust temperature around 300 K. Subsequently, Iqbal et al. (2012, 2014), using the continuous-time random-walk Monte Carlo technique, showed that  $H_2$  production could have meaningful efficiency up to 700 K, depending upon the depth of the chemisorption well. Apart from  $H_2$  formation, a Fischer-Tropsch-based synthesis has been used in solar nebular conditions to form hydrocarbons from the reaction between CO and  $H_2$ , as catalyzed by iron and nickel in meteors (Kress & Tielens 2001). For high-temperature regions such as those surrounding protostars, gas-phase networks have been extended to temperatures up to 800 K (Harada et al. 2010), although little has been done to extend the surface chemistry into the chemisorption regime, which should commence at dust temperatures over 100 K, when all physisorbed species begin to thermally desorb appreciably.

The goal of the work discussed in this article is to include surface chemistry occurring via both the LH and ER mechanisms at surface temperatures as high as 400 K, and to incorporate the additional surface chemistry processes into our large simulation of interstellar chemistry in warm regions. One problem with this approach is the lack of experimental studies of chemisorption on surfaces other than transition metals. Generally, it is believed that interstellar dust grains are mostly carbonaceous or siliceous. Therefore, it is pertinent to use available laboratory measurement/theoretical calculations for graphite or silicates to understand the formation of simple molecules in astrophysical environments where dust temperature can be high. We use existing data wherever available and estimate values when not available for the sake of completeness. For this work, we considered graphite, which has been a mimic for carbonaceous grains, and for which there are more available data than for silicate grains. Although there will be different types of sites available on graphite, which might lead to a variety of binding energies for each individual molecule, as a first step we considered a single type of binding site for the chemisorbed species considered, similar to the low-temperature grain-surface chemistry, which involves one type of physisorption site. In Section 2, we discuss the binding energies for chemisorbed molecules and summarize available measurements. We introduce a simple estimate for species for which there are no measurements. In Section 3, we discuss the types of physical and chemical processes that are included in our study. Our chemical network is discussed in Section 4 followed by results in Section 5. Finally, in Section 6, we draw our conclusions.

## 2. Chemisorption Binding Energies on Graphite

The term binding energy for adsorbed species is often used to refer to desorption from the surface as well as accretion onto the surface. When molecules are bound to a surface by weak physisorption forces, there is no formal difference between the energy given off during adsorption or the energy needed for desorption; one can use the term binding energy for each, although the sign for adsorption energy can be negative, depending upon convention. For chemisorption, there is often an activation energy involved in adsorption. Detailed balance suggests that this activation energy also be considered in desorption. Given the number of uncertainties in the desorption energies on graphite due to

**Table 1**  
Binding Energies for Desorption ( $E_{\text{des}}$ ) (eV) and Heats of Formation  $\Delta H_f(\text{gas})$  (kcal mol<sup>-1</sup>) for Chemisorbed Species

Species	$E_{\text{des}}$	Comments	$\Delta H_f(\text{gas})^a$
H	0.935	Zecho et al. (2002)	52.10
$H_2$	1.15	Zecho et al. (2004)	0.0
O	2.50 0.985–1.33	Jelea et al. (2004; higher for defect sites) Moròn et al. (2010)	59.55
OH	0.523	Jelea et al. (2004)	9.32
$O_2$	0.029 2.60	Moròn et al. (2010; ML physisorbed value) defect site	0.0
$H_2O$	0.117	Jelea et al. (2004; physisorbed value)	-57.80
$CH_4$	1.13	Liu et al. (2012)	-17.89
CO	1.21	Marchon et al. (1988; 300 K value)	-26.42
$CO_2$	1.17	Marchon et al. (1988; 300 K value) CO and $CO_2$ values 2–3 times higher when $T > 800$ K	-94.05
HCO	1.21	same as CO	10.40
C	1.79	estimated ( $1/2 \times \text{C-C bond strength}$ )	171.29
$C_2$	1.79	estimated ( $1/2 \times \text{C-C bond strength}$ )	200.22
CH	1.79	estimated ( $1/2 \times \text{C-C}$ ) bond strength, assumed bonded vertically with C atom closest to the graphite, H atom bonding is ignored	142.00
CCH	1.91	estimated [ $1/2 \times (2/3 \times \text{C-C} + 1/3 \times \text{H-C})$ ]	114.0
$CH_2$	2.02	estimated [ $1/2 \times (1/3 \times \text{C-C} + 2/3 \times \text{H-C})$ ]	93.35
$C_2H_2$	1.97	estimated [ $1/2 \times (1/2 \times \text{C-C} + 1/2 \times \text{H-C})$ ]	54.19
$C_2H_3$	2.00	estimated [ $1/2 \times (2/5 \times \text{C-C} + 3/5 \times \text{H-C})$ ]	71.00
$C_2H_4$	2.02	estimated [ $1/2 \times (1/3 \times \text{C-C} + 2/3 \times \text{H-C})$ ]	12.54
$C_2H_5$	2.04	estimated [ $1/2 \times (2/7 \times \text{C-C} + 5/7 \times \text{H-C})$ ]	28.4
$CH_3$	2.05	estimated [ $1/2 \times (1/4 \times \text{C-C} + 3/4 \times \text{H-C})$ ]	34.8
N	1.58	estimated $1/2 \times \text{C-N}$	112.97
NH	1.58	estimated $1/2 \times \text{C-N}$	90.0
$NH_2$	1.95	estimated [ $1/2 \times (1/3 \times \text{N-C} + 2/3 \times \text{H-C})$ ]	45.5
$NH_3$	2.00	estimated [ $1/2 \times (1/4 \times \text{N-C} + 3/4 \times \text{H-C})$ ]	-10.98
NO	1.72	estimated [ $1/2 \times (1/2 \times \text{N-C} + 1/2 \times \text{O-C})$ ]	21.58
HCN	1.58	same as N	32.3
CN	1.69	estimated [ $1/2 \times (1/2[\text{N-C} + \text{C-C}])$ ]	104.0

**Notes.** Some of the listed values were actually obtained for adsorption but can be used for desorption as well because the uncertainty in the desorption energy is greater than the activation energy, which is included for adsorption.

<sup>a</sup> Surface heat of formation can be determined by subtracting the desorption energy from the gaseous heat of formation.

measurement and theoretical techniques or estimation, and the nature of the surface, as well as the small size of the activation energy compared with the binding energy, we ignore this term.

We will label the desorption energy, the adsorption energy, and the activation energy for adsorption for a given species  $A$  by  $E_{\text{des},A}$ ,  $E_{\text{ads},A}$ , and  $E_{a,A}$  respectively. It is to be noted that in the chemical and surface science literature, these energies are also described by  $Q$ 's. Therefore,  $E$ 's and  $Q$ 's may be treated as synonymous in this context. The labels for diffusion barrier and activation energy for a reaction between two surface species  $A$  and  $B$  are  $E_{\text{diff},A}$ ,  $E_{\text{diff},B}$ , and  $E_{a,AB}$ , respectively, while the bond energy for a gaseous diatomic species is represented by the symbol  $D_{AB}$ . For more complex reactions, this parameter can be equated to the exothermicity of reaction, typically computed for desorbed species. The barrier against diffusion is, as with physisorption, assumed to be a fraction of the desorption energy. The fraction used here is 0.5. The terms “adsorption” and “accretion” are often used synonymously, while the terms “desorption” and “binding” are also used in such a manner.

Table 1 contains the desorption energies on graphite for all chemisorbed species in our network in units of eV. Some physisorbed species are also listed because they can be produced by exothermic reaction of chemisorbed species. For example, physisorbed water can be produced due to the reaction between chemisorbed H and OH. The physisorbed species will desorb immediately upon formation except at the lowest temperatures. Gaseous heats of formation are also given so that surface heats of formation can be determined.

We first discuss desorption energies based on experimental and theoretical values then introduce our approximate method. Reactions with atomic hydrogen on low-temperature surfaces are of great importance, such as in the formation of methanol. A similar importance can be assumed for chemisorbed atomic hydrogen at higher temperatures. The chemisorption of atomic hydrogen on graphite has been studied both computationally and experimentally by several groups (Ferro et al. 2002, 2003; Sha & Jackson 2002; Zecho et al. 2002, 2004; Allouche et al. 2005; Sha et al. 2005; Kerwin & Jackson 2008; Arrou et al. 2011; Karlický et al. 2014). The computational study of hydrogen adsorption on graphite is mostly done using density functional theory (DFT). It was found that H atoms can form a bond with a carbon atom on the graphite surface with a binding energy of  $\sim 0.7$  eV. It was also found that to make such a bond, carbon atom puckering out of the surface plane is necessary, leading to a barrier of 0.2–0.3 eV. Zecho et al. (2002) found that the desorption energy is coverage dependent. In particular, they measured the desorption energy to be 0.6 eV from a leading edge by analysis of the results of temperature programmed desorption, although when the coverage is low (1/8 monolayer) they found this energy to rise to 1.27 eV. Therefore, we used a value of 0.935 eV, which is the average between these two values. Subsequently, Zecho et al. (2004) found that the activation energy for thermal desorption for deuterium decreases from 1.1 eV at low coverage to 0.6 eV near saturation. Ideally, one should probably use a coverage-dependent binding energy, but it is difficult to obtain such a relationship. The desorption energy of  $D_2$  was also measured by Zecho et al. (2004) and Allouche et al. (2005). We took a value of 1.150 eV for  $H_2$ , assuming that the two isotopomers have roughly the same desorption energy (Zecho et al. 2004).

Several authors have studied the adsorption of chemisorbed oxygen atoms (Kelemen & Freund 1985; Incze et al. 2001, 2003; Jelea et al. 2004; Moròn et al. 2010). Using experimental measurements, Kelemen & Freund (1985) found the adsorption energy of oxygen to vary between 2.52 and 3.69 eV depending upon coverage and type of binding, e.g., edge sites. Jelea et al. (2004) calculated the interaction of hydrogen and oxygen atoms with graphite using the density functional formalism. We took their oxygen (O) and hydroxyl (OH) radical adsorption energies, which are 2.50 eV and 0.523 eV, respectively, from these authors, who also calculated the activation energies for the formation of OH and  $H_2O$  with the diffusive (LH) and ER mechanisms. Although Moròn et al. (2010) quoted a lower adsorption energy for O than Jelea et al. (2004), we used the value from Jelea et al. (2004), mainly because most authors (Kelemen & Freund 1985; Incze et al. 2001, 2003) quoted a higher value compared with Moròn et al. (2010) and it is also closer to the experimental value. We took the adsorption energy of 1.13 eV for  $CH_4$  from Liu et al. (2012). There is strong evidence, however, that methane only physisorbs to graphite, as do all alkanes through 10 carbon atoms, although the experiment from which this result comes was undertaken on a graphite film (Tait et al. 2006). For CO and  $CO_2$ , the adsorption energies, taken from Marchon et al. (1988), are 1.21 eV and 1.17 eV, respectively, and correspond to their room temperature values. These energies are higher by 2–3 times when the temperature is above 800 K.

The desorption energies of other species in the chemisorption network are in the main estimated crudely in the following manner, which is based on the idea that chemisorption occurs onto individual C atoms (Klose 1992). First consider an atom X landing upon a carbon atom of the graphite C. If we can ignore all other atoms, then a single bond  $X \rightarrow C$ , or more simply,  $X-C$ , will be formed. But the graphite surface around the carbon atom will be disrupted and some of the bonding strength of the C atom to other atoms will be lessened. The net result will be that the adsorption of atom X leads to a system binding (desorption) energy less than the energy of the single bond  $X-C$ . To estimate this binding energy, we assume crudely that the carbon network loses an amount of energy equal to half of the standard  $X-C$  bond, so that the overall binding energy of the X atom to the system is half that of the single bond. This assumption can be tested against experimental values for oxygen and hydrogen atoms on graphite. For O, the strength of the O–C single bond is known to be 3.71 eV, so our assumption leads to a desorption energy for O of 1.85 eV, somewhat lower than the chosen experimental value of 2.5 eV. Now consider the case of atomic hydrogen. The H–C single-bond energy is 4.28 eV, so we obtain a desorption energy of 2.14 eV, which is somewhat greater than the binding energy used of 0.935 eV. So, our estimate for the binding energy of atomic adsorbates on graphite is probably useful to only  $\pm 1$  eV. Extending this approximation to atomic carbon leads to a binding energy of 1.79 eV based on the energy of 3.86 eV for a C–C single bond.

We next turn to molecular adsorbates, starting with  $C_2$ . If this species lands vertically, we can assume that we need only consider the binding energy of the lower carbon atom, so that we obtain a binding energy of 1.79 eV for this species. If



diatomic carbon lies horizontally, we do not add the two  $1/2$  C–C single bonds but average them with weighting factors of 0.5 so that the result still remains the same. We thus ignore the possibility that more than one single bond exists between adsorbate and graphite, an obvious oversimplification, but likely more reasonable than simple addition for smaller species. The complexity of the issue, however, is illustrated by experiments concerning the adsorption of acetone on both graphite and nanotubes. On nanotubes, the binding energy is large while on graphite there is only physisorption (Chakrapani et al. 2003).

Now let us consider hydrocarbon adsorbates. If the H atoms on the adsorbate hydrocarbon are directed away from the graphite, then we will not account for them in computing the adsorption energy. On the other hand, if the H atoms lie close to the graphite structure, we will account for them in a similar manner to our horizontal  $C_2$  calculation. For CH, we assume the CH to be bonded vertically with the C atom closest to the graphite, then the H atom can be ignored, and we once again have a desorption energy of 1.793 eV. For CCH, a linear molecule, it is also unclear whether the adsorbate lies horizontally or vertically. Let us assume it lies horizontally. In that case, we propose that the desorption energy involves both  $1/2$  of the C–C bond (3.586 eV) and  $1/2$  of the H–C bond (4.28 eV) with weighting according to the number of atoms, so that we get a desorption energy of  $1/2 \times [2/3 \times 3.586 \text{ eV} + 1/3 \times 4.28 \text{ eV}] = 1.91 \text{ eV}$ , whereas the vertical structure would lead to 1.79 eV. We have used a value of 1.91 eV for CCH. The  $CH_2$  molecule has an isosceles triangle structure and can attack the graphite bond with the carbon in the forefront. If so, the desorption energy will be 1.79 eV. If the H atoms bond partially to the graphite, we use a formula similar to that for CCH but with  $1/3$  weight for C–C and  $2/3$  weight for H–C, i.e.,  $1/2 \times [1/3 \times 3.586 \text{ eV} + 2/3 \times 4.28 \text{ eV}] = 2.02 \text{ eV}$ . We use this latter value. If a horizontal position is assumed for  $C_2H_2$ , which is a linear molecule, the one bond to the carbon in graphite can be divided equally between carbon and hydrogen atoms, which leads to  $1/2 \times [1/2 \times 3.586 \text{ eV} + 1/2 \times 4.28 \text{ eV}] = 1.97 \text{ eV}$ , the value used in our calculations. For  $CH_3$ , the position of the methyl atop the graphite is somewhat unclear, so we assume a flat horizontal structure with a  $3/4$  weight for H–C and a  $1/4$  weight for C–C to get 2.05 eV for the desorption energy. This value is used despite the fact that it is significantly higher than the experimental result from the Yates group (Mandeltort et al. 2012) for a Li-treated surface. The chosen desorption energy for  $CH_4$  is 1.13 eV (Liu et al. 2012) rather than a much lower value of 0.15 eV, which clearly represents a physisorbed state (Tait et al. 2006). For the calculated value, we would have to assume that one of the hydrogens is bonded to the graphitic carbon, which would lead to  $1/2(H-C)$  or 2.14 eV, about double the chosen value. For the  $C_2H_3$  molecule, we also assume a planar or near-planar configuration so that the  $1/2$  bond from the graphite is divided among the two C–C bonds and the three H–C bonds to give a desorption energy of 2.00 eV. The final molecule of the series is  $C_2H_4$ , which is a planar molecule and lies atop the graphite structure. The weighting here is  $1/3$  for the carbons and  $2/3$  for the hydrogens, leading to a desorption energy of 2.02 eV (the same as for  $CH_2$  assuming it lies horizontally).

We have followed a similar treatment for species of the type  $NH_n$ , in which the C–C bond is replaced by the N–C bond,

which has a strength of 3.16 eV, thus  $1/2 \times N-C$  will be 1.58 eV. The desorption energies for N, NH,  $NH_2$ , and  $NH_3$  are 1.58, 1.58, 1.954, and 2 eV respectively. For NO, if the configuration is horizontal, we have  $1/2 \times [1/2 \times (N-C) + 1/2 \times (O-C)] = 1.73 \text{ eV}$  and considering the vertical configuration with O nearest the graphite, we get  $1/2 O-C$ , or  $1/2 \times N-C = 1.85 \text{ eV}$ , the same as for the calculated value for O.

For the case of HCO, we assume a vertical structure with the O bonding to the graphite, as is likely to be the case for CO. The CO desorption energy was found to be 1.214 eV by Marchon et al. (1988) at room temperature; this value increases by a factor of 2–3 times above 800 K. A vertical structure for O–C (O on the bottom and so attaching to the graphitic carbon) means that its desorption energy should be the same as for O (1.85 eV), which is the case only when we take the high-temperature values. We, therefore, assume that the H contributes little and that the desorption energy for HCO should be around the same as for CO, i.e., 1.214 eV, the value used for our calculations, rather than the purely “theoretical” value.

The last two species to be considered are CN and HCN. Assuming that N is the lowest atom in a vertical structure, we obtain the estimated desorption energy for HCN to be the same as for atomic nitrogen, or 1.58 eV, the same as for CN if it is vertical and N is on the bottom. If CN lies horizontally, we average the N–C and C–C bond strengths to obtain 1.69 eV. If one compares our calculated values for the following molecules— $CH_4$ , CO, and  $CO_2$ —with the values used in Table 1, we see that a better assumption for our estimated binding energies would involve  $1/3$  of an X–C bond rather than  $1/2$ . Given the uncertainties in our estimated desorption energies, model calculations with the values halved will also be performed to determine the sensitivity of calculated abundances to uncertain desorption energies.

### 3. Processes Involved in Chemisorption

We now provide a framework for the inclusion of chemisorbed species into astrochemical modeling. Similar to diffusive grain-surface chemistry via physisorption, diffusive chemistry via chemisorption also takes place in four primary steps: adsorption, diffusion, reaction, and desorption. The chemistry via the ER process does not require diffusion because the gas-phase species adsorbs atop the reactant adsorbate. In Figure 1, various related physical and chemical processes for three molecules A, B, and AB are shown; these processes are discussed in the subsequent subsections. Note that we used the letter s for surface, although we are only considering chemisorption in this figure, for which we could also use the letter c.

#### 3.1. Adsorption and Sticking

Adsorption of a chemisorbed species onto a grain surface can occur indirectly via a physisorption site or directly to a chemisorption site, if they exist. Any species can be initially physisorbed and, in the presence of a large barrier to a chemisorption site, remain in physisorption sites although only at low temperatures is the time before desorption large enough for reactions to occur. A physisorbed species can proceed to a chemisorbed site without lateral transfer provided it can overcome this barrier or if it can travel laterally to a

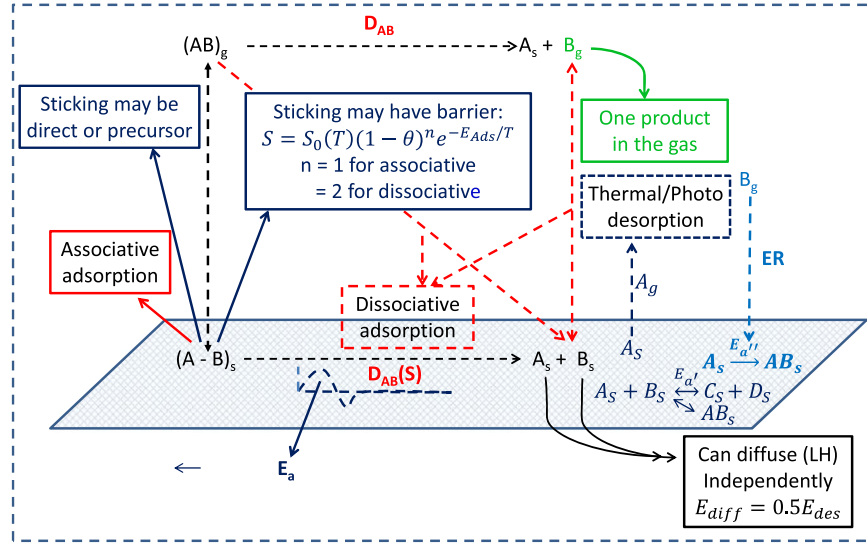


**Figure 1.** Schematic diagram showing various processes connected with the chemistry occurring via chemisorption. Dashed arrows with dashed boxes are used to represent a process; e.g., associative and dissociative adsorption, thermal desorption and photodesorption, Eley–Rideal (ER) reaction mechanism, etc. while comments are included with solid arrows and solid boxes.

chemisorption site, a process known as precursor-mediated adsorption. This barrier may be submerged below the initial gas-phase energy, which leads to non-activated adsorption, or it can also lie above it, so that vertical adsorption, which requires tunneling, or sufficient thermal energy can occur, a process known as activated adsorption. Direct adsorption occurs if the incoming species falls directly into a chemisorption site, which can occur if physisorption sites lie at different environments on the surface, which appears to be the case for graphite. Direct associative adsorption to a chemisorption site is shown in Figure 1; here, a gas-phase species,  $(AB)_g$ , lands on the surface and remains intact. As it approaches the surface, the species can also totally or partially dissociate, a process referred to as dissociative adsorption. This process is also shown in the figure. Dissociative adsorption, not considered here, is more strongly associated with transition metal surfaces where it can represent 100% of the adsorption, especially for catalytic surfaces. A detailed discussion can be found in Kolasinski (2002). In this work, we assume that only associative adsorption occurs. Other processes shown in the figure include two types of chemical reactions: one in which two species ( $A_s$  and  $B_s$ ) react and one in which a bond is broken in  $AB_s$  to form two products  $A_s$  and  $B_s$  on the surface with an endothermicity given by  $D_{AB}(S)$ , the surface bonding energy. The activation energies for the bond-breaking endothermic process and the reaction to form  $C_s$  and  $D_s$  are  $E_a$  and  $E_{a'}$ , respectively, where the subscript “*reac*” has been omitted.

The rate of adsorption ( $s^{-1}$ ) of a given gas-phase species  $A$  in the absence of an activation barrier can be calculated using the following equation:

$$r_{ads,A} = S_A \sigma_g v_A n_d, \quad (1)$$

where  $S_A$  is the sticking coefficient,  $\sigma_g$  is the granular cross section ( $cm^2$ ),  $v_A$  is the velocity ( $cm s^{-1}$ ), and  $n_d$  is the dust particle number density ( $cm^{-3}$ ). Although reality is doubtless more complex, two simple formulae exist for the sticking coefficient—one for associative adsorption and one for dissociative adsorption.

For associative adsorption, the equation is

$$S_A = S_{0,A}(1 - \theta), \quad (2)$$

where  $\theta$  is the fractional coverage of the surface, which for chemisorption is normally limited to a maximum of one monolayer. For the case of dissociative adsorption, the formula is

$$S_A = S_{0,A}(1 - \theta)^2. \quad (3)$$

For both equations, it is assumed that  $S_{0,A} = 1$ . Because barriers to adsorption are normal in chemisorption, the formula for the sticking coefficient and thus the rate of adsorption is multiplied by the Boltzmann factor  $\exp(-E_{a,A}/T)$ , where  $E_{a,A}$  is the activation energy for adsorption. For graphite, we initially use an activation barrier for adsorption of 0.3 eV. We also ran models with lower activation energies to understand its role.

### 3.2. Diffusion and Reaction

A chemisorbed species can react via both the diffusive (LH) and ER mechanisms, discussed in the introduction. The LH mechanism for chemisorbed species is treated in the same approximate manner that Hasegawa et al. (1992) treated diffusive reactions via physisorption. The first-order rate coefficient of reaction ( $s^{-1}$ ) is then given by the equation

$$k_{AB} = \kappa_{AB}(r_{diff,A} + r_{diff,B}), \quad (4)$$

where  $r_{diff,A}$  and  $r_{diff,B}$  are the rates of diffusion for species  $A$  and  $B$  over a whole grain, which in turn are related to the classical hopping rate, e.g.,

$$r_{hop,A} = \nu_0 \exp(-E_{diff,A}/T_d), \quad (5)$$

which is defined as the hopping rate from one potential minimum (site) to an adjacent one. The rate of diffusion is the hopping rate divided by the number of sites on a grain  $N_d$ ,

which is approximately  $10^6$  for a grain of radius  $0.1 \mu$ . Here,  $T_d$  is the dust temperature,  $\nu_0$  is the trial frequency, which can be an order of magnitude or so larger than the analogous value used for physisorption, and  $E_{\text{diff},A}$  is the hopping barrier for the species  $A$ , sometimes called the diffusion barrier (Hasegawa et al. 1992). The energy barrier for hopping is a critical parameter, which ideally should be measured in the laboratory. In standard physisorption treatments, it is treated as a fraction of the desorption energy. Here we follow this prescription and assume that the value of the fraction is 0.5. The  $\kappa_{AB}$  factor arises from the presence of a chemical activation energy barrier and can be approximated by the quantum mechanical tunneling probability or the hopping probability, whichever is greater. A more detailed treatment has been advocated by Herbst & Millar (2008). Normally, the tunneling possibility is considered through the use of a simple rectangular potential although once again more detailed treatments are available.

For chemisorption, we have included an activation barrier for every reaction in addition to the diffusion barrier. If we assume that the products remain on the surface, most of our included reactions are associative or dissociative:



and



The activation barrier for the associative process, which mainly leads to the formation of an additional bond, can be estimated with the equation (Shustorovich 1988):

$$E_{a,AB} = E_{\text{des},A}E_{\text{des},B}/(E_{\text{des},A} + E_{\text{des},B}) \quad (8)$$

or with

$$E_{a,AB} = E_{\text{des},AB} + D_{AB} - (E_{\text{des},A} + E_{\text{des},B}), \quad (9)$$

whichever is greater in magnitude (Shustorovich 1988). The alternate equation is rarely the larger. Once  $AB_s$  is formed, it can desorb back to the gas partially depending upon the efficiency of reactive desorption. The activation energy for Equation (7), which primarily breaks a bond, can be estimated using the equation (Shustorovich 1988):

$$E_{a,AB} = E_{\text{des},AB} + D_{AB} + E_{\text{des},A} \\ \times E_{\text{des},B}/(E_{\text{des},A} + E_{\text{des},B}) - (E_{\text{des},A} + E_{\text{des},B}), \quad (10)$$

or an equivalent equation in which the  $D_{AB}$  term incorporates the desorption terms of reactants and products. This activation energy can also be applied to thermal dissociation processes, which are discussed later in the text. These are assumed to be first order, like the Polanyi–Wigner equation for thermal desorption.

We have also included the ER mechanism, for which we utilized the treatment of Ruaud et al. (2015) in which the rate ( $\text{cm}^{-3} \text{s}^{-1}$ ) is given by the expression

$$r_{AB} = n_B \sigma v_A n(A) n_d, \quad (11)$$

where  $n_B$  is the average fraction of the granular surface occupied by species  $B$ ,  $n(A)$  is the volume density of gaseous species  $A$ ,  $n_d$  is the volume density of dust, and  $\sigma$  is the granular cross section. We have assumed that reactive collisions between the gaseous species and the adsorbate

possess a nonzero activation energy barrier of 0.2 eV based on some laboratory work, but those involving atomic hydrogen and selected radical–radical processes are barrier free.

### 3.3. Desorption Processes

Once species are formed on the surface, they can desorb into the gas phase via thermal and nonthermal desorption processes. The thermal desorption rate ( $r_{\text{des}}$ ) per molecule is given by the first-order Polanyi–Wigner equation:

$$r_{\text{des}} = \nu_0 \exp(-E_{\text{des}}/T_d), \quad (12)$$

where the desorption energies are given in Table 1. Because of the magnitude of  $E_{\text{des}}$ , thermal desorption will only be effective at much higher temperatures than encountered for physisorbed species. For example, at our highest studied temperature of 400 K, the thermal desorption rate of a species with a desorption energy of 20,000 K (1.724 eV) will contain a negative exponent of  $-50$  leading to an exponential factor of  $\approx 10^{-22}$ . We therefore include several nonthermal desorption terms, which are analogous to those used in gas/grain simulations for physisorbed species.

The first is reactive desorption, in which the exothermicity of reaction is channeled into the desorption of products. We treat reactive desorption from chemisorbed species via the standard formula of Garrod et al. (2007) for the fraction  $f$  of desorbed products:

$$f = aP/(1 + aP), \quad (13)$$

where  $P$  is the probability that the system has enough energy to desorb in the relevant vibrational coordinate for bond-surface breaking, while  $a$  is an empirical parameter relating the frequency of desorption to the frequency of relaxation of the exothermicity of reaction into the bulk of the grain. Although the probability  $P$  can be obtained from the Rice–Ramsperger–Kessel (RRK) formula (Garrod et al. 2007), it is so close to unity for physisorption that the formula for  $f$  reduces to  $a$ , which is called the efficiency and is normally set to 0.01. For chemisorbed products, the greater desorption energy leads to a greater vibrational frequency, which is comparable to the frequency of relaxation, so we set  $a$  equal to unity, and the formula for the desorption probability reduces to

$$f = P/(1 + P). \quad (14)$$

Moreover, the probability of gaining sufficient energy to desorb can be much smaller than unity, due to the increased desorption energy, in which case  $f \approx P$ . To obtain a value for  $P$ , we must consider two cases. In the first case, the exothermicity of the reaction exceeds the desorption energy, a case similar to physisorbed products although the two energies are closer; therefore, we can use the RRK formula in Garrod et al. (2007; see their Equation (1)). In the second case, the energy needed for desorption exceeds the exothermicity of reaction, so that additional energy is needed for thermal desorption. This energy can only come from thermal energy, so we crudely estimate the probability of obtaining sufficient energy for desorption to be a Boltzmann factor akin to the Polanyi–Wigner equation:

$$P = \exp(-\epsilon/T_d), \quad (15)$$

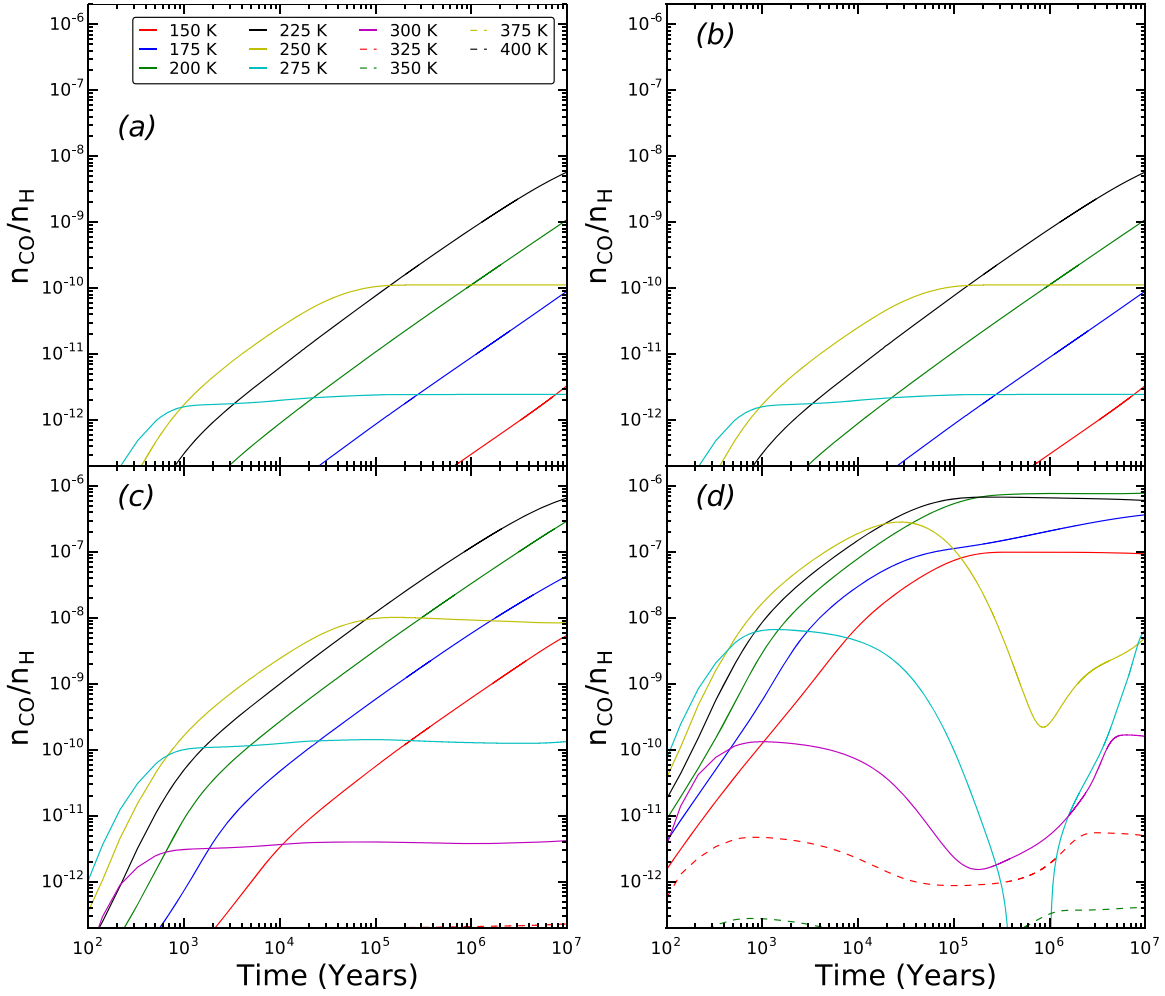


**Figure 2.** Fractional abundances of chemisorbed CO as a function of time for all four sets of models. Each panel contains the results of 11 isothermal models for temperatures between 150 and 400 K with 25 K intervals. Results for Sets 1, 2, 3, and 4 are shown in panels (a), (b), (c), and (d), respectively.

**Table 2**  
Low Metal Elemental Abundances in Initial Forms Used for Various Models with Respect to Total Hydrogen

Elements	He	C <sup>+</sup>	N	O	F	Si <sup>+</sup>
abundances	0.09	7.3(−5)	2.14(−5)	1.76(−4)	1.8(−8)	8(−9)
Elements	S <sup>+</sup>	Fe <sup>+</sup>	Na <sup>+</sup>	Mg <sup>+</sup>	Cl <sup>+</sup>	P <sup>+</sup>
abundances	8(−8)	3(−9)	2(−9)	7(−9)	1(−7)	2(−10)

where

$$\epsilon = E_{\text{des}} - E_{\text{exo}}. \quad (16)$$

A temperature of 400 K was utilized. For the case of two products, we added their desorption energies. An upper limit for  $P$  of 0.1 was used to constrain overly high values for small species.

The second process is photodesorption by cosmic-ray-generated UV photons and external UV photons (Öberg et al. 2008, 2009a, 2009b). The photodesorption yield for physisorption is measured to be at most  $10^{-3}$  (Öberg et al. 2008, 2009a, 2009b), whereas for chemisorption we considered an order of magnitude lower yield, i.e.,  $10^{-4}$ , due to the stronger binding and consequent need for higher-energy photons. The yield  $Y_{\text{pd}}$  can be converted into a photodesorption rate for a

given species in terms of the flux of incoming radiation and the cross-sectional area per adsorbed species (Öberg et al. 2008, 2009a, 2009b). Finally, based on the paper of Hasegawa & Herbst (1993), we included nonthermal desorption via the heating of grains by cosmic-ray bombardment, although due to the high binding energy of chemisorbed species, we expect only a very small effect.

### 3.4. Photodissociation and Thermal Dissociation

We have included photodissociation for chemisorbed species, due to cosmic-ray-generated UV photons and external UV photons. The photodissociation cross sections are mainly from gas-phase measurements and estimates, and it is quite likely that they are too large for the more heavily bound chemisorbed species.



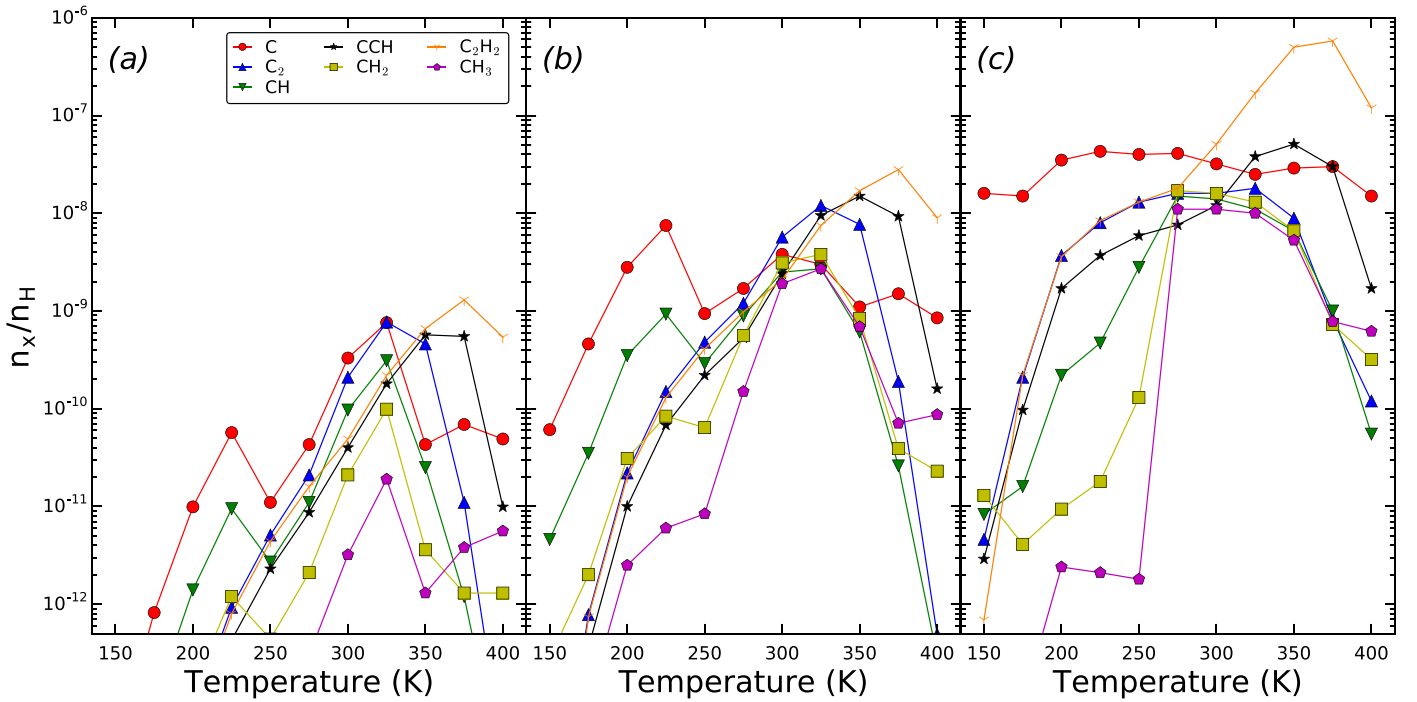


**Figure 3.** Fractional peak abundances for C and assorted carbonaceous molecules as a function of temperature. Results for Sets 1, 3, and 4 are shown in panels (a), (b), and (c), respectively.

**Table 3**  
Description of Various Isothermal Models

Models	Binding Energy	Temperature	Adsorption Barrier
Set 1	Binding energies listed in Table 1	150–400 with 25 K interval	0.3 eV
Set 2	Binding energies estimated in Table 1 halved	Same as Set 1	0.3 eV
Set 3	Same as Set 1	Same as Set 1	0.2 eV
Set 4	Same as Set 1	Same as Set 1	0.1 eV

We have also included thermal dissociation, a thermal surface process akin to thermal desorption, but in this case, the bond that is broken is not the surface-adsorbate bond but a bond between portions of the molecule. The first-order rate coefficient for this process is approximated by the equation

$$k_{\text{th,diss}} = \nu' \exp(-E_a/T_d), \quad (17)$$

where  $E_a$  is the activation energy for the dissociation, defined in Equation (10), and  $\nu'$  is set equal to the characteristic frequency of both desorption and diffusion (Hasegawa et al. 1992). For both photodissociation and thermal dissociation, products remain on the surface.

#### 4. Chemical Network

The set of reactions involving chemisorption in some manner is listed in the Appendix. It can be seen that attention is given to smaller species because they are dominant, with the largest ones involving two carbon atoms. The major reactions are between atoms and small molecules, in close analogy with the reactions that occur between physisorbed species at 10 K. In this case, both the binding energies and the diffusion barriers are larger than their 10 K counterparts. These reactions and their rate coefficients are inserted into our gas-grain reaction

network, discussed previously in Acharyya & Herbst (2017), which is based both on the latest KIDA collection of gas-phase reactions (Wakelam et al. 2014), and the Garrod et al. (2008) collection of grain-surface reactions, although the low-temperature surface reactions other than those involving atomic hydrogen are only useful for warm-up models. We used a two-phase model, which does not distinguish between the surface and the bulk of the ice mantle for temperatures sufficiently low that mantles exist. At higher temperatures, where chemisorption dominates, the mantle consists of one surface layer at most. We have included 27 chemisorbed species and approximately 425 reactions involving these species. Dust particles are assumed to be the classical particles of radius  $10^{-5}$  cm. The role of size distributions, as kindly brought up by the referee, will be considered in a future paper.

The so-called low metal elemental abundances shown in Table 2 are used here. The table also shows their initial ionization stages. All values presented are fractional abundances with respect to total hydrogen, and the initial abundance of hydrogen is assumed to be molecular. The abundances of elemental fluorine and chlorine are taken from Acharyya & Herbst (2017), and all others are from Wakelam & Herbst (2008).



**Table 4**  
Peak Abundances of Assorted Chemisorbed Species for Set 1 Isothermal Models

Species	150 K	175 K	200 K	225 K	250 K	275 K	300 K	325 K	350 K	375 K	400 K
H-c	6.7(−10)	5.4(−09)	3.8(−11)	7.5(−13)	3.1E-14)	2.3E-15)	2.6E-16)	3.9E-17)	7.3E-18)	1.8E-18)	5.6E-19)
H <sub>2</sub> -c	7.5(−42)	2.2(−36)	1.9(−37)	2.8(−38)	5.4E-39)	6.4E-39)	4.8E-38)	2.2E-37)	9.2E-39)	2.1E-38)	5.7E-38)
O-c	1.0(−12)	3.0(−11)	3.7(−10)	2.1(−09)	5.6E-09)	6.5E-09)	6.2E-09)	5.5E-09)	5.1E-09)	4.8E-09)	4.6E-09)
OH-c	4.7(−22)	3.5(−23)	5.7(−24)	1.3(−24)	2.5E-25)	2.5E-26)	3.8E-27)	7.2E-28)	3.3E-28)	3.5E-28)	3.9E-28)
O <sub>2</sub> -c	1.0(−99)	1.0(−99)	5.7(−73)	9.0(−65)	1.4E-58)	4.2E-54)	1.7E-50)	1.6E-47)	5.9E-45)	1.0E-42)	9.4E-41)
H <sub>2</sub> O-c	4.9(−27)	2.6(−28)	2.0(−31)	1.6(−33)	2.2E-35)	2.5E-37)	6.2E-39)	2.4E-40)	1.2E-41)	1.1E-42)	1.4E-43)
CH <sub>4</sub> -c	2.9(−17)	8.4(−17)	9.6(−16)	1.6(−15)	1.2E-17)	2.9E-19)	4.6E-20)	9.8E-21)	5.3E-22)	2.0E-22)	8.3E-23)
CO-c	3.4(−12)	9.1(−11)	1.1(−09)	5.8(−09)	1.1E-10)	2.5E-12)	1.0E-13)	6.9E-15)	6.8E-16)	8.8E-17)	1.4E-17)
CO <sub>2</sub> -c	8.5(−15)	2.7(−13)	3.6(−12)	3.6(−12)	8.4E-14)	3.0E-15)	1.8E-16)	1.7E-17)	2.1E-18)	3.3E-19)	6.4E-20)
HCO-c	6.4(−32)	9.3(−32)	1.4(−31)	1.9(−31)	1.5E-33)	1.9E-34)	4.3E-34)	9.5E-34)	1.4E-33)	2.3E-33)	2.8E-33)
C-c	3.2(−14)	8.2(−13)	9.9(−12)	5.7(−11)	1.1E-11)	4.3E-11)	3.3E-10)	7.6E-10)	4.3E-11)	6.9E-11)	4.9E-11)
C <sub>2</sub> -c	1.0(−18)	1.1(−15)	7.3(−14)	9.3(−13)	5.1E-12)	2.1E-11)	2.1E-10)	7.7E-10)	4.6E-10)	1.1E-11)	2.9E-14)
CH-c	3.5(−15)	9.8(−14)	1.4(−12)	9.5(−12)	2.7E-12)	1.1E-11)	9.7E-11)	3.1E-10)	2.5E-11)	1.2E-12)	1.6E-14)
CCH-c	6.4(−19)	5.3(−16)	3.4(−14)	4.3(−13)	2.3E-12)	8.7E-12)	4.0E-11)	1.8E-10)	5.7E-10)	5.5E-10)	9.9E-12)
CH <sub>2</sub> -c	2.9(−16)	8.6(−15)	1.4(−13)	1.2(−12)	4.4E-13)	2.1E-12)	2.1E-11)	9.9E-11)	3.6E-12)	1.3E-12)	1.3E-12)
C <sub>2</sub> H <sub>2</sub> -c	1.7(−19)	1.1(−15)	6.6(−14)	8.0(−13)	4.4E-12)	1.6E-11)	4.9E-11)	2.2E-10)	6.6E-10)	1.3E-09)	5.4E-10)
C <sub>2</sub> H <sub>3</sub> -c	4.6(−22)	2.5(−18)	1.7(−16)	2.2(−15)	2.8E-16)	1.4E-16)	1.1E-17)	1.2E-18)	1.4E-19)	2.6E-20)	4.9E-21)
C <sub>2</sub> H <sub>4</sub> -c	7.4(−22)	1.8(−20)	1.4(−18)	2.0(−17)	2.2E-18)	2.4E-18)	4.0E-19)	3.4E-20)	6.2E-21)	1.2E-21)	3.4E-22)
CH <sub>3</sub> -c	2.0(−17)	6.3(−16)	1.2(−14)	1.2(−13)	5.8E-14)	3.0E-13)	3.2E-12)	1.9E-11)	1.3E-12)	3.8E-12)	5.6E-12)
C <sub>2</sub> H <sub>5</sub> -c	1.4(−29)	3.6(−29)	7.6(−28)	2.7(−27)	3.1E-27)	1.0E-26)	2.4E-25)	4.9E-25)	1.1E-24)	5.2E-24)	1.5E-23)
N-c	6.7(−14)	1.8(−12)	2.2(−11)	1.5(−10)	6.9E-10)	2.2E-09)	4.4E-09)	4.7E-10)	2.9E-11)	2.0E-12)	1.7E-13)
NH-c	1.2(−14)	3.4(−13)	4.5(−12)	3.5(−11)	1.7E-10)	5.8E-10)	2.1E-10)	2.6E-13)	4.9E-15)	9.3E-16)	1.1E-16)
NH <sub>2</sub> -c	1.9(−15)	6.3(−14)	9.6(−13)	9.0(−12)	5.0E-11)	2.1E-10)	7.5E-11)	3.2E-12)	3.8E-12)	1.1E-12)	1.5E-14)
NH <sub>3</sub> -c	1.3(−16)	4.7(−15)	8.4(−14)	9.4(−13)	5.8E-12)	2.8E-11)	1.5E-11)	1.7E-12)	2.9E-12)	2.4E-12)	3.3E-13)
NO-c	6.6(−17)	2.0(−15)	2.7(−14)	2.2(−13)	1.3E-12)	4.0E-12)	8.5E-12)	8.2E-12)	4.1E-12)	1.5E-12)	1.7E-13)
CN-c	6.0(−17)	1.8(−15)	1.9(−14)	1.3(−13)	7.1E-13)	3.3E-12)	1.9E-11)	1.0E-11)	6.7E-13)	6.7E-14)	5.9E-14)
HCN-c	3.2(−16)	9.4(−15)	9.8(−14)	6.9(−13)	3.7E-12)	1.7E-11)	8.5E-11)	4.2E-11)	2.8E-12)	2.5E-13)	3.0E-14)

**Note.** The suffix -c is used to denote that the species are chemisorbed.

## 5. Results

Two types of models have been run, isothermal and warm up. Our isothermal models can be best characterized as models with gas-phase chemistry and chemisorption chemistry. These models are designed to understand the effect of chemisorption on the production of simple molecules at temperatures high enough that physisorption is not important. Each model is run at a fixed temperature between 150 and 400 K with an interval of 25 K. The gas and dust temperatures are the same. We used a density of  $1 \times 10^5 \text{ cm}^{-3}$ , a visual extinction of 10 mag, and a cosmic-ray ionization rate ( $\zeta$ ) of  $1.3 \times 10^{-17} \text{ s}^{-1}$ . All the other parameters are kept the same as for a standard cold dense cloud core. In the warm-up models, designed to represent the formation of hot cores, we followed the two-phase physical model prescribed by Brown et al. (1988). In the first phase, the cloud undergoes isothermal collapse at 10 K, from a density of 3000 to  $10^7 \text{ cm}^{-3}$  in  $\approx 10^6$  yr, during which the visual extinction grows from 1.64 to 432 mag. In the second phase, the collapse is halted, and the temperature is increased linearly from 10 to 400 K over three timescales:  $10^6$ ,  $2 \times 10^6$ , and  $5 \times 10^6$  yr. We kept both the gas and dust temperature equal to each other during the warm-up phase. All abundances are relative to the total hydrogen and for a chemisorbed species unless mentioned otherwise.

In discussing our calculated fractional abundances for chemisorbed species, we assume that the advent of the *James Webb Space Telescope* (JWST) with its high sensitivity may allow the detection of chemisorbed species down to a fractional abundance lower than the limit in current studies of

physisorbed surface species of approximately one monolayer, or with standard parameters, a fractional abundance of roughly  $10^{-6}$  with respect to total hydrogen. This corresponds to 100% coverage in our models, and so represents a maximum for chemisorption, which is restricted to one monolayer. It is possible that the sensitivity of JWST might permit the detection of a minimum abundance an order of magnitude lower, so that a fractional coverage of 0.1 monolayers or a fractional abundance of  $10^{-7}$  would be detectable if the IR spectra of species chemisorbed on graphite would be studied in more detail. This assessment, however, rests on the possibility that the detection of chemisorption can be distinguished from and not overwhelmed by infrared physisorption spectra from the same species or from more abundant physisorbed species detected at lower temperatures. One obvious method of distinction would be the high dust temperatures that only support chemisorption, although most high-temperature sources are accompanied by lower temperatures so that both a favorable geometry and an observable frequency difference between chemisorbed and physisorbed species should exist. Such a frequency difference is likely, although its size may not be very large. Consider the case of CO. A study of physisorbed CO on graphite yields the standard interstellar frequency of  $2140 \text{ cm}^{-1}$  (Boyd et al. 2002), while studies of CO chemisorbed on assorted metals show a range of IR frequencies from 1870 to  $2104 \text{ cm}^{-1}$  (Pritchard et al. 1975; Yates et al. 1979). We are not aware of studies of the IR spectrum of CO chemisorbed on graphite. Indirect detection of chemisorption by gas-phase detection of desorbed products might affect the limit on sensitivity.

**Table 5**  
Peak Abundances of Assorted Chemisorbed Species for Set 2 Isothermal Models

Species	150 K	175 K	200 K	225 K	250 K	275 K	300 K	325 K	350 K	375 K	400 K
H-c	6.7(−10)	5.4(−09)	3.8(−11)	7.5(−13)	3.1(−14)	2.3(−15)	2.6(−16)	3.9(−17)	7.3(−18)	1.8(−18)	5.6(−19)
H <sub>2</sub> -c	7.5(−42)	2.2(−36)	1.9(−37)	2.4(−38)	4.1(−39)	9.8(−40)	2.9(−40)	2.2(−39)	1.1(−38)	4.7(−38)	1.4(−37)
O-c	1.0(−12)	3.0(−11)	3.7(−10)	2.1(−09)	5.6(−09)	6.5(−09)	6.2(−09)	5.5(−09)	5.1(−09)	4.8(−09)	4.6(−09)
OH-c	4.7(−22)	3.5(−23)	5.7(−24)	1.3(−24)	2.5(−25)	2.5(−26)	3.8(−27)	7.2(−28)	3.3(−28)	3.5(−28)	3.9E-28)
O <sub>2</sub> -c	1.0(−99)	1.0(−99)	5.7(−73)	9.0(−65)	1.4(−58)	4.2(−54)	1.7(−50)	1.6(−47)	5.9(−45)	1.0(−42)	9.4(−41)
H <sub>2</sub> O-c	4.9(−27)	2.6(−28)	2.0(−31)	1.6(−33)	2.2(−35)	2.5(−37)	6.1(−39)	2.4(−40)	1.2(−41)	1.1(−42)	1.4(−43)
CH <sub>4</sub> -c	2.9(−17)	8.4(−17)	6.4(−16)	9.0(−16)	1.2(−17)	2.9(−19)	2.0(−20)	2.0(−21)	5.3(−22)	2.0(−22)	8.3(−23)
CO-c	3.4(−12)	9.1(−11)	1.1(−09)	5.8(−09)	1.1(−10)	2.5(−12)	1.0(−13)	7.0(−15)	6.8(−16)	8.8(−17)	1.4(−17)
CO <sub>2</sub> -c	8.5(−15)	2.7(−13)	3.6(−12)	3.6(−12)	8.4(−14)	3.0(−15)	1.8(−16)	1.7(−17)	2.1(−18)	3.3(−19)	6.4(−20)
HCO-c	6.4(−32)	9.3(−32)	1.4(−31)	1.9(−31)	1.5(−33)	1.9(−34)	4.3(−34)	9.5(−34)	1.4(−33)	2.3(−33)	2.8(−33)
C-c	3.2(−14)	7.5(−14)	2.2(−14)	6.2(−16)	2.6(−17)	2.4(−18)	2.9(−19)	4.5(−20)	1.1(−20)	2.7(−21)	8.5(−22)
C <sub>2</sub> -c	1.0(−18)	4.4(−16)	2.2(−17)	1.1(−18)	5.5(−20)	3.8(−21)	2.1(−22)	4.0(−23)	9.0(−24)	1.9(−24)	4.6(−25)
CH-c	3.5(−15)	2.3(−15)	2.2(−17)	1.4(−18)	6.2(−20)	3.1(−21)	3.7(−22)	5.4(−23)	8.9(−24)	1.8(−24)	6.0(−25)
CCH-c	6.4(−19)	5.3(−16)	8.6(−16)	8.1(−17)	4.3(−18)	2.5(−19)	2.4(−20)	4.1(−21)	7.6(−22)	1.5(−22)	4.3(−23)
CH <sub>2</sub> -c	2.9(−16)	3.4(−16)	1.1(−16)	2.9(−16)	3.8(−17)	1.9(−18)	3.0(−19)	4.1(−20)	6.3(−21)	1.7(−21)	5.5(−22)
C <sub>2</sub> H <sub>2</sub> -c	1.7(−19)	1.1(−15)	3.4(−14)	1.9(−15)	6.9(−17)	4.3(−18)	3.9(−19)	5.5(−20)	1.0(−20)	2.3(−21)	7.4(−22)
C <sub>2</sub> H <sub>3</sub> -c	4.6(−22)	2.5(−18)	1.4(−17)	3.0(−18)	4.4(−19)	4.2(−20)	6.2(−21)	1.3(−21)	2.6(−22)	7.6(−23)	2.2(−23)
C <sub>2</sub> H <sub>4</sub> -c	7.4(−22)	1.8(−20)	1.3(−19)	1.0(−20)	1.5(−22)	5.8(−24)	1.0(−24)	2.4(−25)	1.1(−25)	5.3(−26)	3.3(−26)
CH <sub>3</sub> -c	2.0(−17)	3.3(−17)	6.4(−18)	9.9(−19)	3.6(−20)	2.4(−21)	2.6(−22)	1.0(−22)	6.2(−23)	2.2(−23)	6.9(−24)
C <sub>2</sub> H <sub>5</sub> -c	1.4(−29)	3.6(−29)	5.6(−28)	1.8(−29)	1.6(−31)	5.4(−33)	5.5(−34)	1.1(−34)	4.0(−35)	3.7(−35)	3.2(−35)
N-c	4.6(−14)	1.5(−15)	3.0(−17)	1.4(−18)	1.1(−19)	1.5(−20)	2.7(−21)	6.6(−22)	2.0(−22)	6.8(−23)	2.7(−23)
NH-c	1.1(−15)	1.8(−18)	2.8(−22)	1.4(−23)	2.2(−24)	8.5(−25)	2.7(−25)	1.3(−25)	6.0(−26)	3.3(−26)	1.8(−26)
NH <sub>2</sub> -c	2.4(−16)	1.6(−16)	1.9(−18)	1.3(−20)	4.4(−22)	1.4(−22)	2.4(−23)	2.7(−24)	7.3(−25)	2.8(−25)	1.4(−25)
NH <sub>3</sub> -c	2.0(−17)	6.4(−17)	4.5(−17)	5.9(−19)	1.9(−20)	1.1(−21)	1.6(−22)	1.8(−23)	4.3(−24)	1.5(−24)	6.3(−25)
NO-c	6.6(−17)	5.9(−17)	7.0(−19)	2.3(−20)	1.4(−21)	2.8(−22)	7.9(−23)	3.2(−23)	1.5(−23)	7.1(−24)	3.5(−24)
CN-c	5.5(−17)	3.3(−17)	3.7(−17)	1.8(−18)	8.1(−20)	6.7(−21)	8.1(−22)	1.2(−22)	1.8(−23)	6.1(−24)	1.6(−24)
HCN-c	3.1(−16)	1.2(−16)	1.6(−18)	6.0(−20)	4.6(−21)	6.1(−22)	1.1(−22)	3.1(−23)	1.5(−23)	7.7(−24)	4.4(−24)

**Note.** The suffix -c is used to denote that the species are chemisorbed.

### 5.1. Isothermal Models

Four sets of isothermal models, as listed in Table 3, were run to understand the impact of chemisorption on the formation of molecules. In Set 1, the binding energies used for desorption are the same as shown in Table 1, and the barrier for adsorption is set at 0.3 eV, the fiducial value. In Set 2, those binding energies that were estimated, i.e., those lying physically below CO<sub>2</sub> in Table 1, were halved. In Sets 3 and 4, we used the desorption energies described in Table 1 but the barrier against adsorption was reduced to 0.2 and 0.1 eV, respectively.

We start our discussion of results with the time evolution of the CO abundance because CO is the most observed molecule. We subsequently discuss the evolution of abundances of species for which reasonably high abundances ( $>10^{-8}$ ) are achieved. These species include NH<sub>3</sub> and C<sub>2</sub>H<sub>2</sub> for Set 3 and Set 4. For all other species, we concentrated mainly on peak abundances. These are listed in Tables 4 (Set 1), 5 (Set 2), 6 (Set 3), and 7 (Set 4) as well as in some figures as functions of temperature. For Set 2, we found that although CO, H, and C, which can drive the chemistry, have similar abundances compared with the Set 1 values due to accretion from the gas phase, the abundances of other chemisorbed species are never as high due to efficient desorption, especially at higher temperatures, owing to the use of lower binding energies for estimated values. In addition to discussions of abundances for the various sets, the time variation of the coverage of the grain surface is discussed for all models.

#### 5.1.1. CO and CO<sub>2</sub>

The chemisorbed CO abundance with respect to total hydrogen as a function of time for Set 1 isothermal models is shown in Figure 2(a). The CO abundance increases monotonically with time up to  $10^7$  yr through a temperature of 225 K primarily due to accretion and the absence of an efficient desorption mechanism. For this range, the higher the temperature, the larger the abundance at any given time, due to the increasing ease of overcoming the adsorption barrier. The highest abundance reached by CO in Set 1 is  $5.8 \times 10^{-9}$ . For models having temperatures of 250 K and above, the abundance of CO reaches a steady-state value well before  $10^7$  yr, with a subsequent slight decrease. The steady-state abundance and the subsequent slight decrease occur primarily because the increase in temperature also increases the thermal desorption rate. For Set 2, shown in Figure 2(b), we see almost no change because for CO, the desorption energy was not decreased. Figures 2(c) and (d), which show the CO abundance for Sets 3 and 4, make it clear that the CO abundance is increased significantly for Set 3, and even more for Set 4. The increase is primarily due to the lowering of the activation barrier for accretion first from 0.3 to 0.2 eV and then to 0.1 eV. The highest abundance for Set 3,  $6.6 \times 10^{-7}$ , occurs at 225 K, whereas for Set 4 its value,  $7.8 \times 10^{-7}$ , is reached at 200 K, both of which should be detectable, as discussed previously.

We found that the reaction between chemisorbed oxygen and carbon is not very efficient in producing chemisorbed CO; rather, the accretion of gas-phase CO is the dominant process for locking CO to a chemisorbed site. However, other

**Table 6**  
Peak Abundances of Assorted Chemisorbed Species for Set 3 Isothermal Models

Species	150 K	175 K	200 K	225 K	250 K	275 K	300 K	325 K	350 K	375 K	400 K
H-c	1.0(−06)	9.7(−07)	2.2(−07)	7.2(−11)	2.4(−12)	1.2(−13)	1.1(−14)	1.3(−15)	1.9(−16)	3.8(−17)	9.7(−18)
H <sub>2</sub> -c	4.2(−36)	7.3(−32)	3.5(−31)	2.2(−34)	2.4(−35)	4.8(−36)	1.5(−35)	1.8(−35)	4.6(−36)	5.1(−36)	3.6(−36)
O-c	1.9(−09)	1.7(−08)	1.0(−07)	3.0(−07)	4.8(−07)	3.7(−07)	2.5(−07)	1.7(−07)	1.2(−07)	9.7(−08)	7.8(−08)
OH-c	4.7(−19)	1.1(−20)	1.4(−21)	1.1(−22)	1.8(−23)	1.4(−24)	1.8(−25)	3.6(−26)	9.8(−27)	7.3(−27)	6.8(−27)
O <sub>2</sub> -c	1.0(−99)	1.0(−99)	4.6(−68)	1.7(−60)	1.0(−54)	1.3(−50)	2.7(−47)	1.5(−44)	3.5(−42)	4.2(−40)	2.7(−38)
H <sub>2</sub> O-c	5.5(−23)	3.5(−24)	1.4(−25)	1.3(−29)	1.2(−31)	7.8(−34)	1.1(−35)	2.2(−37)	7.2(−39)	4.5(−40)	4.4(−41)
CH <sub>4</sub> -c	5.8(−14)	5.5(−14)	1.8(−13)	1.4(−13)	1.1(−15)	1.3(−16)	7.9(−17)	8.1(−18)	2.3(−19)	4.5(−21)	1.6(−21)
CO-c	5.5(−09)	4.4(−08)	3.0(−07)	6.6(−07)	1.0(−08)	1.4(−10)	4.2(−12)	2.3(−13)	1.8(−14)	1.8(−15)	2.5(−16)
CO <sub>2</sub> -c	1.5(−11)	1.3(−10)	9.6(−10)	4.4(−10)	8.0(−12)	1.9(−13)	7.8(−15)	5.4(−16)	5.3(−17)	6.8(−18)	1.1(−18)
HCO-c	5.9(−29)	2.6(−29)	1.1(−27)	1.5(−28)	2.7(−30)	5.1(−32)	1.9(−32)	3.2(−32)	3.6(−32)	4.9(−32)	4.9(−32)
C-c	6.1(−11)	4.6(−10)	2.8(−09)	7.5(−09)	9.4(−10)	1.7(−09)	3.8(−09)	3.0(−09)	1.1(−09)	1.5(−09)	8.5(−10)
C <sub>2</sub> -c	2.1(−15)	7.8(−13)	2.2(−11)	1.5(−10)	4.8(−10)	1.2(−09)	5.7(−09)	1.2(−08)	7.7(−09)	1.9(−10)	4.9(−13)
CH-c	4.6(−12)	3.5(−11)	3.5(−10)	9.3(−10)	2.9(−10)	8.9(−10)	2.5(−09)	2.7(−09)	6.1(−10)	2.6(−11)	2.9(−13)
CCH-c	1.3(−15)	3.6(−13)	1.0(−11)	6.8(−11)	2.2(−10)	5.3(−10)	2.4(−09)	9.5(−09)	1.5(−08)	9.3(−09)	1.6(−10)
CH <sub>2</sub> -c	2.8(−13)	2.0(−12)	3.1(−11)	8.4(−11)	6.4(−11)	5.6(−10)	3.1(−09)	3.8(−09)	8.4(−10)	3.9(−11)	2.3(−11)
C <sub>2</sub> H <sub>2</sub> -c	3.5(−16)	7.4(−13)	2.0(−11)	1.3(−10)	4.1(−10)	9.8(−10)	2.1(−09)	7.5(−09)	1.7(−08)	2.8(−08)	9.0(−09)
C <sub>2</sub> H <sub>3</sub> -c	9.4(−19)	1.6(−15)	5.0(−14)	3.5(−13)	3.3(−14)	8.7(−15)	4.8(−16)	2.4(−16)	2.5(−17)	7.0(−18)	2.9(−19)
C <sub>2</sub> H <sub>4</sub> -c	1.5(−18)	1.0(−17)	4.0(−16)	2.7(−15)	2.1(−16)	1.5(−16)	1.8(−17)	1.1(−18)	1.6(−19)	2.5(−20)	5.9(−21)
CH <sub>3</sub> -c	1.5(−14)	1.0(−13)	2.5(−12)	6.0(−12)	8.4(−12)	1.5(−10)	1.9(−09)	2.7(−09)	6.9(−10)	7.1(−11)	8.7(−11)
C <sub>2</sub> H <sub>5</sub> -c	2.8(−26)	2.5(−26)	2.3(−25)	4.2(−25)	2.9(−25)	5.7(−25)	1.2(−23)	5.4(−23)	3.4(−23)	1.0(−22)	2.5(−22)
N-c	1.3(−10)	1.2(−09)	6.4(−09)	2.3(−08)	5.9(−08)	1.0(−07)	1.4(−07)	1.5(−08)	7.4(−10)	4.2(−11)	3.0(−12)
NH-c	1.8(−11)	1.5(−10)	1.3(−09)	5.0(−09)	1.8(−08)	3.8(−08)	4.3(−08)	1.6(−10)	2.6(−13)	2.0(−14)	2.0(−15)
NH <sub>2</sub> -c	2.3(−12)	1.9(−11)	2.9(−10)	1.3(−09)	1.7(−08)	6.6(−08)	6.0(−08)	3.9(−10)	2.3(−11)	6.2(−12)	2.0(−13)
NH <sub>3</sub> -c	1.0(−13)	9.2(−13)	2.3(−11)	9.4(−11)	2.3(−09)	2.4(−08)	4.5(−08)	1.0(−09)	1.9(−10)	1.1(−10)	5.6(−12)
NO-c	1.2(−13)	1.0(−12)	7.3(−12)	2.6(−11)	9.6(−11)	2.2(−10)	3.4(−10)	2.6(−10)	1.1(−10)	3.1(−11)	2.9(−12)
CN-c	1.2(−13)	1.2(−12)	5.6(−12)	2.1(−11)	6.7(−11)	2.0(−10)	7.6(−10)	3.0(−10)	1.9(−11)	1.7(−12)	1.0(−12)
HCN-c	6.5(−13)	6.4(−12)	3.0(−11)	1.1(−10)	3.5(−10)	1.0(−09)	3.5(−09)	1.3(−09)	6.8(−11)	5.1(−12)	5.2(−13)

**Note.** The suffix -c is used to denote that the species are chemisorbed.

than accretion, chemisorbed CO is produced by breaking the chemisorbed HCO and CO<sub>2</sub> due to photodissociation and via the ER process. Thus, it is clear that if the accretion barrier is low or absent, then the amount of CO locked in chemisorbed sites may be significant and may even be detected.

Like CO, CO<sub>2</sub> is also primarily accreted from the gas-phase species, which can reach a peak abundance of a few times 10<sup>−7</sup>. However, its surface abundance is significantly lower than that of CO. Its fractional abundance exceeds 10<sup>−10</sup> for Sets 3 and 4, with its highest abundance coming for Set 4 at 225 K and having a value of 1.7 × 10<sup>−9</sup>.

### 5.1.2. Carbon and Small Hydrocarbons

Figure 3 depicts peak fractional abundances over the range of times for selected hydrocarbons as functions of temperature for Sets 1, 3, and 4 in panels (a), (b), and (c), respectively. Note that each point on the graph can be expanded into a model with a time axis. Elemental carbon, shown with red circles in Figure 3, is effectively produced by accretion from the gas, reaching relatively large peak abundances for Sets 3 and 4, which can potentially drive a rich organic chemistry, although in this study, we attempted to understand the formation of smaller molecules only. The peak abundance of chemisorbed elemental carbon for Sets 1 and 3 increases with temperature until 225 K but after that does not follow any particular trend. For Set 4, the abundance profile is nearly flat and always remains above 10<sup>−8</sup> for all temperatures, with a highest abundance of 4.3 × 10<sup>−8</sup> for 225 K. Other than accretion from the gas phase, a fraction of chemisorbed C is also formed, due to dissociation of chemisorbed C<sub>2</sub> and CH. We found that C<sub>2</sub>, CH, CCH, CH<sub>2</sub>, C<sub>2</sub>H<sub>2</sub>, and CH<sub>3</sub> are produced with high

abundances exceeding 10<sup>−8</sup>, whereas the highest abundances of CH<sub>4</sub>, C<sub>2</sub>H<sub>3</sub>, C<sub>2</sub>H<sub>4</sub>, and C<sub>2</sub>H<sub>5</sub> lie many orders of magnitude lower. The peak abundances of all these species are listed in Tables 4–7 for Sets 1, 2, 3, and 4, respectively.

The peak abundance of C<sub>2</sub> is shown in Figure 3 with upward-facing triangles. For Set 1, its abundance increases with temperature up to 325 K, for which it has a peak abundance of 7.6 × 10<sup>−10</sup>, after which it decreases. For Sets 3 and 4, the C<sub>2</sub> abundance lies above 10<sup>−10</sup> for all models from 225 to 375 K, and a maximum peak abundance comes at 225 K with a value of 4.3 × 10<sup>−8</sup> for Set 4. It is primarily produced by dissociation of chemisorbed C<sub>2</sub>H, and a smaller fraction is produced by the addition of two chemisorbed carbon atoms. Hydrogenation of chemisorbed elemental carbon produces an abundance of CH above 10<sup>−10</sup> for the Set 1, Set 3, and Set 4 models at several temperatures. Peak abundance comes for Set 4 with a value of 1.5 × 10<sup>−8</sup> at 275 K. Similarly, hydrogenation of chemisorbed C<sub>2</sub> produces C<sub>2</sub>H, which is also produced by the dissociation of C<sub>2</sub>H<sub>2</sub>. Chemisorbed C<sub>2</sub>H shows a peak abundance of 5.1 × 10<sup>−8</sup> for Set 4 at 350 K. Chemisorbed CH<sub>2</sub>, at an early time, is formed by the accretion of gas-phase CH<sub>2</sub> but, at a later time, is formed by the hydrogenation of chemisorbed CH. Its peak abundance comes at 275 K for Set 4 at a value of 1.7 × 10<sup>−8</sup>.

Chemisorbed C<sub>2</sub>H<sub>2</sub> (acetylene) is abundantly formed for several models in Sets 1, 3, and 4 as shown in Figure 3 with a broken orange line, with relatively high efficiency above 200 K. The peak abundance lies at 375 K with a value of 5.8 × 10<sup>−7</sup> for Set 4, which is likely above the *JWST* detection limit for grain-surface species. Its time variation for Sets 3 and 4 is shown in Figures 4(c) and (d), respectively. It can be seen

**Table 7**  
Peak Abundances of Assorted Chemisorbed Species for Set 4 Isothermal Models

Species	150 K	175 K	200 K	225 K	250 K	275 K	300 K	325 K	350 K	375 K	400 K
H-c	2.1(−06)	2.0(−06)	1.1(−07)	6.8(−10)	9.7(−12)	5.3(−12)	4.0(−13)	2.7(−14)	4.4(−15)	7.3(−16)	1.7(−16)
H <sub>2</sub> -c	2.2(−35)	4.2(−31)	1.0(−29)	2.0(−32)	4.0(−34)	7.5(−33)	7.2(−34)	1.0(−34)	7.1(−34)	2.5(−33)	1.2(−33)
O-c	2.1(−07)	4.1(−07)	1.4(−06)	1.6(−06)	2.1(−06)	2.1(−06)	2.0(−06)	2.1(−06)	1.8(−06)	1.4(−06)	1.1(−06)
OH-c	1.7(−18)	5.3(−21)	2.9(−22)	1.6(−23)	3.6(−24)	3.1(−23)	6.7(−24)	1.7(−24)	6.2(−25)	2.9(−25)	2.0(−25)
O <sub>2</sub> -c	1.0(−99)	1.0(−99)	8.7(−66)	4.8(−59)	1.8(−53)	4.2(−49)	1.8(−45)	2.2(−42)	7.3(−40)	8.6(−38)	4.9(−36)
H <sub>2</sub> O-c	2.4(−22)	2.1(−24)	1.7(−26)	1.3(−29)	6.8(−32)	7.4(−31)	5.8(−33)	7.7(−35)	3.0(−36)	1.9(−37)	3.0(−38)
CH <sub>4</sub> -c	2.0(−11)	3.0(−12)	6.6(−12)	2.9(−12)	8.1(−14)	9.5(−14)	3.1(−15)	2.4(−16)	3.4(−17)	1.4(−18)	3.6(−20)
CO-c	1.0(−07)	3.7(−07)	7.8(−07)	6.8(−07)	2.8(−07)	6.8(−09)	1.7(−10)	5.5(−12)	4.1(−13)	3.5(−14)	4.4(−15)
CO <sub>2</sub> -c	2.1(−11)	7.8(−10)	9.4(−10)	1.7(−09)	3.6(−10)	6.5(−12)	2.2(−13)	1.3(−14)	1.1(−15)	1.2(−16)	1.6(−17)
HCO-c	3.1(−29)	3.0(−29)	5.9(−28)	3.4(−28)	1.7(−28)	1.3(−28)	2.7(−30)	1.1(−30)	9.9(−31)	1.1(−30)	8.9(−31)
C-c	1.6(−08)	1.5(−08)	3.5(−08)	4.3(−08)	4.0(−08)	4.1(−08)	3.2(−08)	2.5(−08)	2.9(−08)	3.0(−08)	1.5(−08)
C <sub>2</sub> -c	4.6(−12)	2.1(−10)	3.7(−09)	8.0(−09)	1.3(−08)	1.6(−08)	1.6(−08)	1.8(−08)	8.9(−09)	8.2(−10)	1.2(−10)
CH-c	8.3(−12)	1.6(−11)	2.2(−10)	4.7(−10)	2.8(−09)	1.5(−08)	1.4(−08)	1.1(−08)	6.6(−09)	1.0(−09)	5.5(−11)
CCH-c	2.9(−12)	9.7(−11)	1.7(−09)	3.7(−09)	5.9(−09)	7.6(−09)	1.2(−08)	3.8(−08)	5.1(−08)	3.0(−08)	1.7(−09)
CH <sub>2</sub> -c	1.3(−11)	4.1(−12)	9.4(−12)	1.8(−11)	1.3(−10)	1.7(−08)	1.6(−08)	1.3(−08)	6.6(−09)	7.3(−10)	3.2(−10)
C <sub>2</sub> H <sub>2</sub> -c	6.9(−13)	2.2(−10)	3.6(−09)	8.4(−09)	1.3(−08)	1.8(−08)	5.1(−08)	1.7(−07)	5.0(−07)	5.8(−07)	1.2(−07)
C <sub>2</sub> H <sub>3</sub> -c	8.7(−16)	7.8(−14)	2.1(−12)	7.9(−12)	4.6(−12)	2.2(−12)	6.3(−13)	7.4(−14)	2.5(−14)	3.5(−15)	9.8(−17)
C <sub>2</sub> H <sub>4</sub> -c	1.5(−15)	1.5(−15)	9.3(−15)	1.4(−14)	1.6(−14)	1.0(−12)	7.8(−15)	7.9(−17)	9.4(−18)	5.4(−19)	1.0(−19)
CH <sub>3</sub> -c	7.9(−14)	9.6(−14)	2.4(−12)	2.1(−12)	1.8(−12)	1.1(−08)	1.1(−08)	1.0(−08)	5.3(−09)	7.8(−10)	6.2(−10)
C <sub>2</sub> H <sub>5</sub> -c	2.2(−23)	2.5(−24)	2.2(−23)	1.3(−23)	5.8(−24)	4.4(−22)	5.0(−21)	1.2(−20)	1.1(−20)	4.0(−21)	2.9(−21)
N-c	3.8(−08)	6.4(−08)	2.7(−07)	2.8(−07)	3.9(−07)	3.8(−07)	3.6(−07)	1.9(−07)	1.8(−08)	9.1(−10)	5.5(−11)
NH-c	8.6(−12)	7.3(−11)	1.2(−09)	1.3(−08)	7.8(−08)	1.2(−07)	1.0(−07)	1.1(−08)	1.2(−10)	7.0(−13)	3.6(−14)
NH <sub>2</sub> -c	9.9(−14)	6.2(−13)	5.7(−12)	5.2(−10)	1.9(−08)	2.1(−07)	1.8(−07)	5.5(−08)	6.0(−10)	8.9(−12)	9.5(−13)
NH <sub>3</sub> -c	1.2(−13)	2.8(−13)	1.2(−12)	1.6(−12)	2.7(−10)	3.2(−07)	5.7(−07)	8.8(−07)	8.3(−08)	2.6(−09)	7.9(−11)
NO-c	4.2(−12)	1.1(−11)	4.3(−11)	4.1(−11)	1.1(−10)	5.7(−09)	1.0(−08)	5.2(−09)	1.9(−09)	5.4(−10)	4.4(−11)
CN-c	2.2(−10)	4.7(−10)	1.3(−09)	1.9(−09)	2.6(−09)	3.4(−09)	3.8(−09)	1.8(−09)	1.0(−09)	2.9(−10)	2.4(−11)
HCN-c	1.2(−09)	2.5(−09)	7.0(−09)	1.0(−08)	1.4(−08)	1.8(−08)	2.1(−08)	1.1(−08)	1.3(−09)	8.7(−11)	9.4(−12)

**Note.** The suffix -c is used to denote that the species are chemisorbed.

that for temperatures 200 K and above, its abundance is large for wider time ranges. It can also be noted that the peak abundance for C<sub>2</sub>H<sub>2</sub> is gradually shifted to higher temperatures and times. Like CH, at early times, the major source for C<sub>2</sub>H<sub>2</sub> is the accretion of gas-phase C<sub>2</sub>H<sub>2</sub> and then at later stages, the dominant synthetic pathway is the hydrogenation of C<sub>2</sub>H on the grain surface. Once formed, acetylene can be dissociated to produce C<sub>2</sub>H as well by thermal and photodissociation. Finally, CH<sub>3</sub>, which is produced by the hydrogenation of CH<sub>2</sub>, achieves a significant abundance for Sets 3 and 4 for temperatures of 275 K and above.

### 5.1.3. Nitrogenated Species

As shown by circles in Figure 5(a), the peak abundances of chemisorbed elemental nitrogen for Set 1 models lie above the level of  $10^{-10}$  for temperatures from 225 to 325 K, peaking at  $4.4 \times 10^{-9}$ , whereas they are always somewhat lower for Set 2. However, for Set 3 and Set 4 models, for which the accretion barrier is lowered to 0.2 eV and 0.1 eV, respectively, the peak abundances are significantly greater, as can be seen in Figures 5(b) and (c) as well as Tables 6 and 7. The peak abundances are  $1.4 \times 10^{-7}$  (at 300 K) and  $3.9 \times 10^{-7}$  (at 250 K), respectively. Atomic nitrogen is efficiently hydrogenated to produce NH and then NH<sub>2</sub>. A small fraction of NH is formed due to dissociation of NH<sub>2</sub>; similarly, dissociation of NH<sub>3</sub> produces some NH<sub>2</sub>. The variation of peak abundance as a function of temperature for both NH and NH<sub>2</sub> can be seen in Figure 5 (upper and lower triangles). Peak abundances for all four sets of models are listed in Tables 4–7.

Other than atomic nitrogen, we include the nitrogen-containing species NH, NH<sub>2</sub>, NH<sub>3</sub>, NO, CN, and HCN in the

chemisorption network. Let us start with ammonia. The variation in the peak abundance of ammonia as a function of temperature is shown in Figure 5. For models with Set 1 and Set 2 parameters, the peak abundance of ammonia is lower than  $10^{-10}$  for all temperatures. However, the ammonia abundance is significantly higher for Set 3 and Set 4 models for temperatures between 250 and 375 K. In particular, the peak abundance for Set 3 of  $4.5 \times 10^{-8}$  comes at 300 K, whereas for Set 4, it is  $8.8 \times 10^{-7}$  and comes at 325 K. This latter value could be large enough to be detectable as its abundance is close to that of species such as methane and possibly ammonia seen in low-temperature ice mantles. At early times, the production of chemisorbed ammonia is due mainly to the accretion of gas-phase NH<sub>3</sub>, after which production due to the hydrogenation of NH<sub>2</sub> becomes the dominant formation pathway. In panel (a) of Figure 6, we show the rates of the major formation processes of chemisorbed NH<sub>3</sub> at 300 K in Set 4 as percentages of the total formation rate as functions of time. It can be seen that until approximately  $2 \times 10^4$  yr, the accretion of NH<sub>3</sub> is dominant, after which the reaction between chemisorbed atomic hydrogen and chemisorbed NH<sub>2</sub> dominates. A small fraction is also produced via the ER reaction between gas-phase atomic hydrogen and chemisorbed NH<sub>2</sub>. Ammonia is also dissociated to form other species. The time dependences of the chemisorbed ammonia abundance with parameters belonging to Sets 3 and 4 are shown in panels (a) and (b) of Figure 4. These abundances are strongly higher at later times for most temperatures because the intermediate time production of ammonia requires the production of the parent species NH<sub>2</sub> to come first.



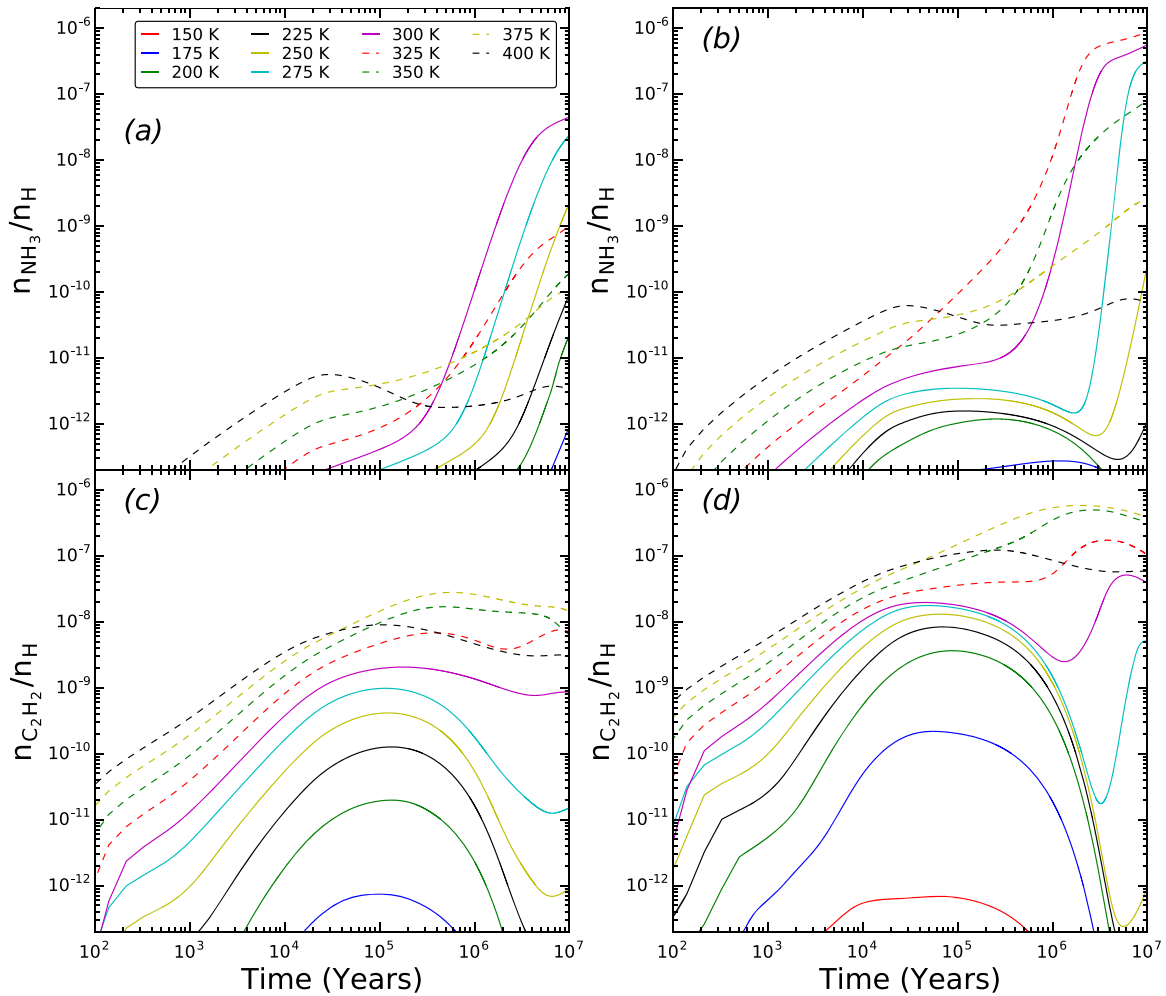


**Figure 4.** Time variation of chemisorbed  $\text{NH}_3$  (top panel) and  $\text{C}_2\text{H}_2$  (bottom panel) abundance for models designated as Set 3 (a and c) and Set 4 (b and d).

The species NO, CN, and HCN are also produced in reasonable quantities for the Set 3 and Set 4 models. For chemisorbed HCN, accretion of gaseous HCN is the dominant formation process at 300 K until the hydrogenation of chemisorbed CN becomes dominant at about  $5 \times 10^5$  yr, as can be seen for Set 4 from panel (b) in Figure 6. The peak HCN abundance can reach up to  $2 \times 10^{-8}$  for the 300 K model in Set 4. The radical CN is produced primarily due to the dissociation of chemisorbed HCN and from the recombination of chemisorbed carbon and nitrogen. It is also accreted from the gas phase. Accretion of NO from the gas phase is the dominant production mechanism for chemisorbed NO followed by the recombination of chemisorbed oxygen and nitrogen. The NO radical is also produced via the ER mechanism, in which a gas-phase atom directly recombines with a chemisorbed one.

#### 5.1.4. Coverage

The time variation at given temperatures of the total surface coverage for the four sets of models is shown in Figure 7. The total coverage is calculated by summing up the abundances of all the chemisorbed species. In the figure, we multiplied the total coverage by 100 to obtain a percentage. For chemisorption, only the first monolayer is allowed; therefore, the

maximum y-axis value for the plot is 100. It is clear from Figures 7(a) and (b) that the total coverage never reaches more than 0.4% for Set 1 and Set 2; thus, chemisorption is relatively unimportant for these two sets. For Set 2, with estimated binding energies reduced to half their values, this change does not influence the overall coverage strongly, showing that the estimated binding energies do not have a significant global influence on the coverage. Nevertheless, the reduction in binding energy decreases overall coverage to a minimum extent and can affect individual molecular abundances more strongly.

Although the overall coverage caused by chemisorption is not very sensitive to our estimated binding energies, it is critically dependent on efficient accretion. Thus, the adsorption barrier plays a more prominent role, and chemisorption is increasingly important when this barrier is reduced, as is evident from Figure 7. In particular, the overall coverage increases up to 40% when the adsorption barrier is reduced to 0.2 eV from 0.3 eV, and to near 100% when the barrier is reduced to 0.1 eV.

At a given temperature, an initial increase in coverage with time is obviously due to accretion, and a near-steady-state condition can be reached. Eventually, a decrease occurs, which is earlier at higher temperatures than at lower ones, due to thermal and nonthermal desorption. In addition, after about  $1 \times 10^5$  yr, the gas-phase abundances for several species start

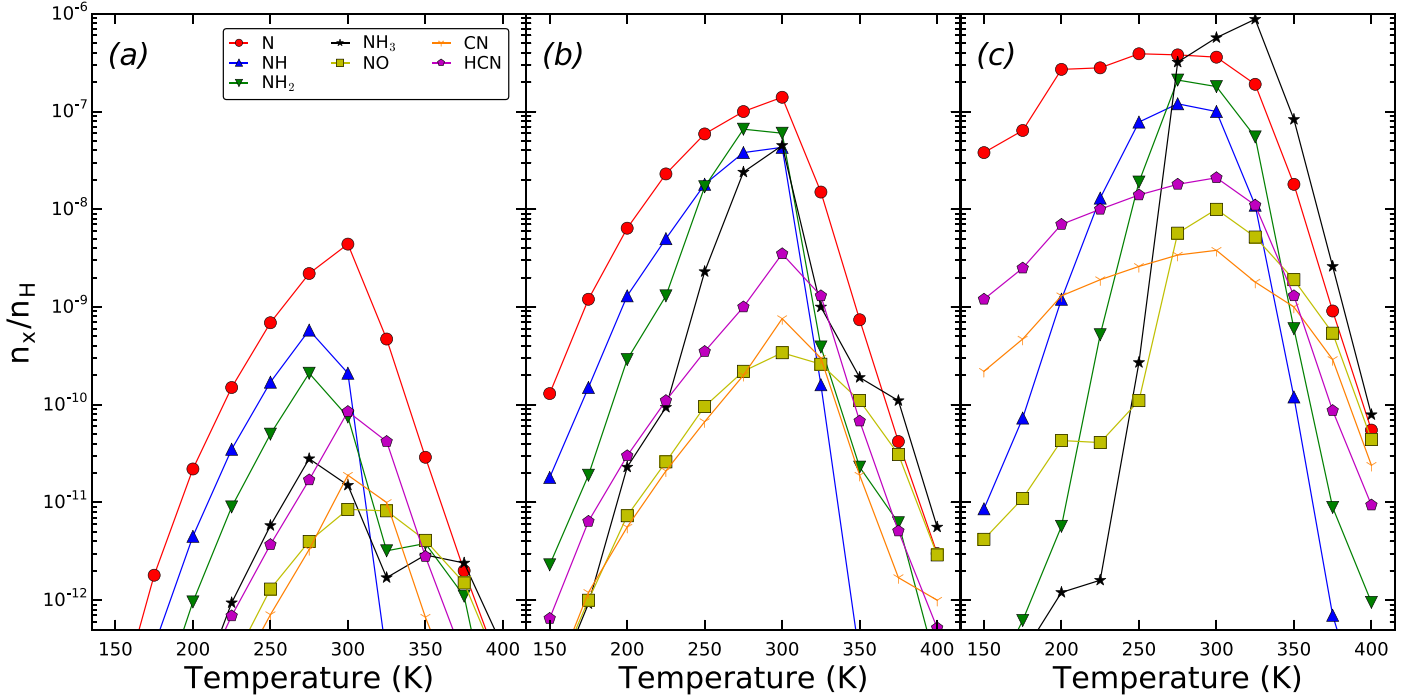


**Figure 5.** Fractional peak abundances for N and assorted nitrogen-containing species as a function of dust temperature. Results for Sets 1, 3, and 4 are shown in panels (a), (b), and (c), respectively.

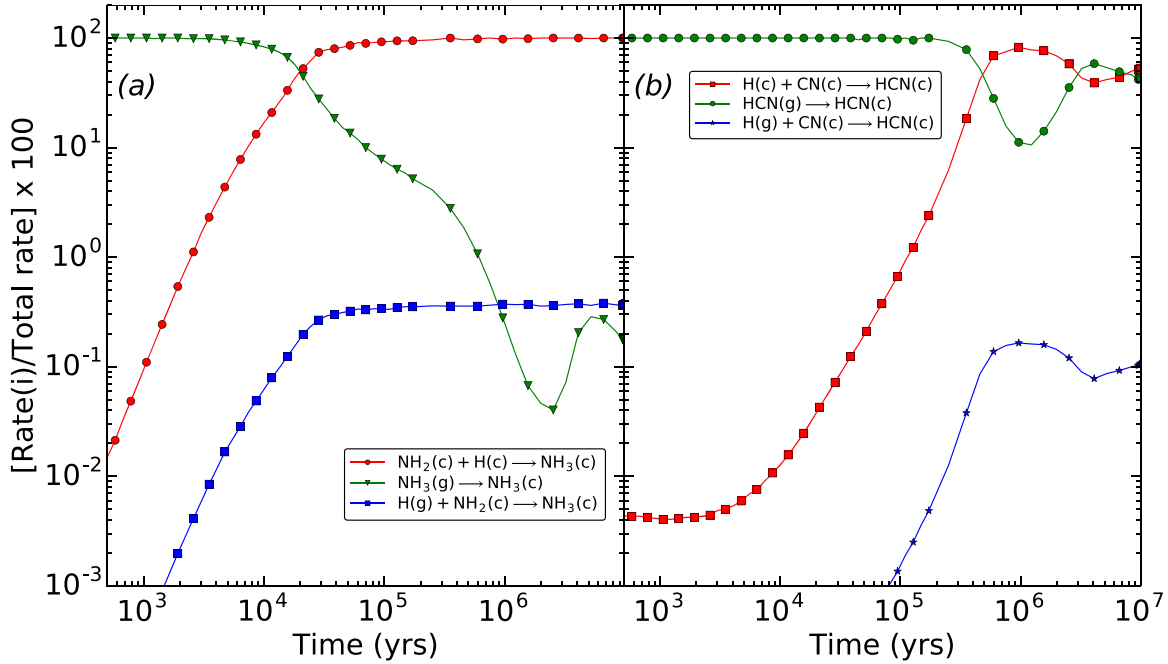


**Figure 6.** Dominant formation processes as percentages of total rate for chemisorbed  $\text{NH}_3$  (panel a) and chemisorbed  $\text{HCN}$  (panel b) are shown for the 300 K isothermal model for Set 4. Chemisorbed species are denoted by (c) and gas-phase species by (g).

to decrease, which will also reduce the accretion and disturb the rather complex balance.

### 5.2. Comparison with Gas-phase Abundances

Figure 8 compares the gas-phase abundances of a species with its chemisorbed abundance for assorted temperatures.

We considered four species that have reasonably higher chemisorbed abundances from Set 4, which has the lowest activation energy for adsorption. It is clear from Figure 8(a) that the gas-phase CO abundance is always significantly higher than its chemisorbed abundance. Thus, the chemisorbed CO will probably cause no change in overall CO gas-phase abundance when desorbed back to the gas phase.

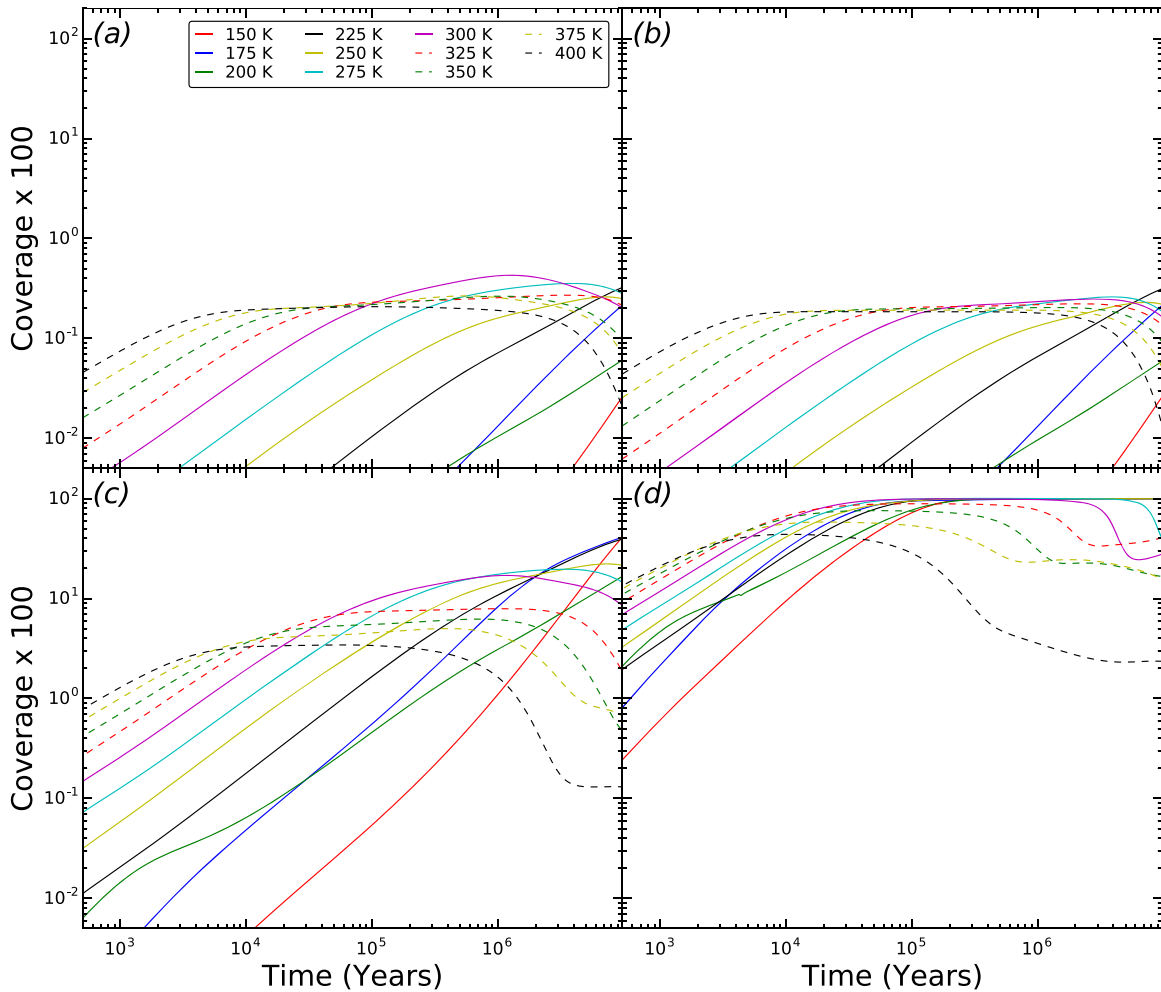


**Figure 7.** Coverage  $\times 100$  is plotted vs. time as a function of dust temperature for all model sets. Panels (a), (b), (c), and (d) exhibit the coverage for Sets 1–4, respectively.

However, for  $\text{C}_2\text{H}_2$  (Figure 8(b)), above  $10^6$  yr, the chemisorbed abundance at 300, 325, 350, and 375 K is higher than the corresponding gas-phase abundance. In that situation, chemisorbed  $\text{C}_2\text{H}_2$  can by desorption add to the gas-phase abundance at certain temperatures; also, some of the loss of the gas-phase  $\text{C}_2\text{H}_2$  can be attributed to accretion onto a chemisorbed site. Figure 8(c) shows the time variation for the gas-phase and chemisorbed  $\text{NH}_3$ . The abundance of chemisorbed  $\text{NH}_3$  can be significantly higher above  $5 \times 10^4$  yr for those models having a temperature between 250 and 375 K. The unusually large abundances of chemisorbed ammonia presumably reflect a combination of slow desorption and rapid formation, the latter due to a rapid surface hydrogenation of  $\text{NH}_2$ . For these models, similar to the case of acetylene, chemisorbed  $\text{NH}_3$  can significantly influence the gas-phase abundance of ammonia in the presence of efficient desorption mechanisms, or some of the large abundance of chemisorbed ammonia could have come from the accretion of the gas, especially at early time. Finally, chemisorbed HCN has a considerably smaller abundance than the gas-phase abundance. Thus, it is unlikely to influence the overall abundance of HCN as is the case for chemisorbed CO. Therefore, it can be concluded that for some species and for certain temperature ranges, chemisorption will have a

reasonably large impact; i.e., it can keep the species locked on the surface and can also alter gas-phase abundances when the species desorb back to the gas phase.

### 5.3. Warm-up Models

As mentioned in Section 5, we employed a two-era warm-up approach, and in the second era, the temperature is increased linearly from 10 to 400 K for three timescales:  $10^6$ ,  $2 \times 10^6$ , and  $5 \times 10^6$  yr. For each timescale, we ran three models having chemisorption adsorption barriers of 0.3, 0.2, and 0.1 eV, respectively. We did not run any models with reduced binding energy as in our isothermal models, because we confined attention to the two most efficient models. The abundance variation of selected chemisorbed species is shown in Figure 9. We primarily discuss models having a warm-up time of  $2 \times 10^6$  yr and adsorption barriers of 0.1 (solid lines) and 0.2 eV (dashed lines).

Figure 9(a) shows the time variation of chemisorbed CO,  $\text{CH}_4$ ,  $\text{CO}_2$ , and NO for these two adsorption barriers during the warm up. All four species reach abundances above  $1 \times 10^{-8}$  for both models. The abundance of chemisorbed CO is particularly high, reaching around  $10^{-6}$ , which makes this species among the more likely to be detected by upcoming facilities such as *JWST* although its peak abundance does not

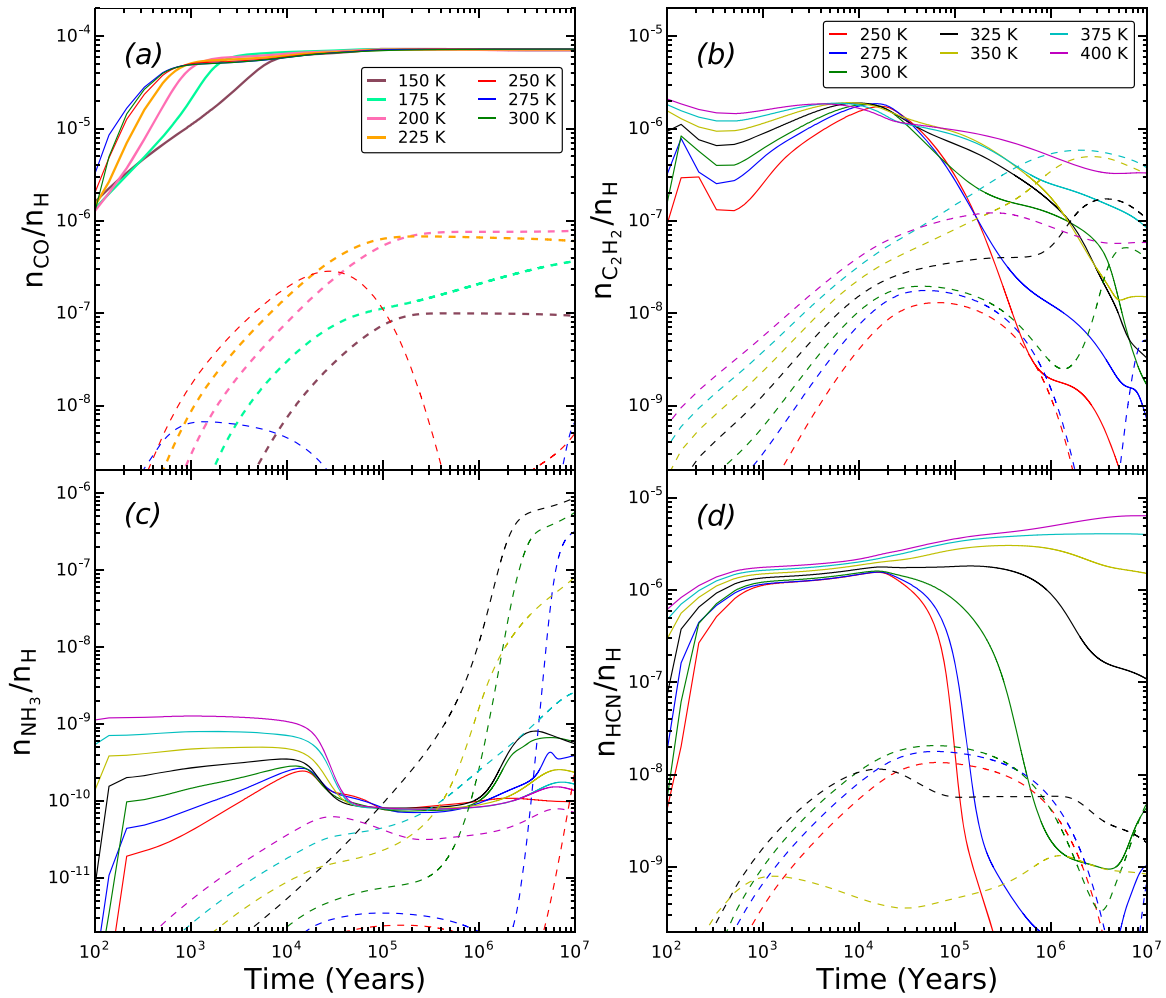


**Figure 8.** Comparison between gas-phase (solid lines) and chemisorbed abundances (dashed lines) for CO (a),  $C_2H_2$  (b),  $NH_3$  (c), and HCN (d). The legends are the same for (b), (c), and (d).

last for a long period of time. Despite this high predicted abundance for chemisorbed CO, the gas-phase abundance of CO versus time is unlikely to change significantly as gaseous CO is very efficiently produced at almost all temperatures, as is evident from Figure 8(a). The peak abundance for the model having an adsorption barrier of 0.2 eV is lower by a factor of 2 for CO and  $CH_4$ , whereas the peak NO and  $CO_2$  abundances are nearly the same. Similarly, Figure 9(b) shows the time variation for the abundances of chemisorbed C,  $C_2$ , CH, and CCH. All four of these species can achieve abundances greater than  $10^{-8}$ , as do the abundances of chemisorbed  $CH_2$ ,  $C_2H_3$ ,  $C_2H_2$ , and  $CH_3$ , shown in Figure 9(c). Of these species, the abundance of chemisorbed  $C_2H_2$  lies between  $10^{-7}$  and  $10^{-6}$  at late times (high temperatures), which can be comparable to its gas-phase abundance; hence, desorption of chemisorbed  $C_2H_2$  can affect the gas-phase abundance at such late times, as can be seen in Figure 8(b). Finally, Figure 9(d) shows the abundances versus time of chemisorbed N, NH,  $NH_2$ , and  $NH_3$ . The abundance of these four species can lie above  $10^{-8}$ , and  $NH_2$  and  $NH_3$  can attain very high abundances near  $10^{-6}$  and, as with  $C_2H_2$ , influence their gas-phase abundances.

Two very significant differences are found between the warm-up models having adsorption barriers of 0.1 and 0.2 eV. With the 0.1 eV barrier, the peak abundance for most species is extended over a smaller time period compared with the 0.2 eV

barrier. In addition, the abundance profiles for the 0.2 eV case are smooth and contain only one peak, whereas with 0.1 eV, the abundances gradually increase initially with time, then attain a near-steady state for some time, then can repeat this process, eventually reaching a flat peak, before decreasing sharply. Thus, there can be multiple steplike structures in the abundance profile. The steplike features are primarily due to the assumption of one monolayer. Initially, at low temperatures, the dominant species is atomic hydrogen; its coverage becomes near 100% between  $1.5 \times 10^6$  and  $1.85 \times 10^6$  yr. The dominance of atomic hydrogen severely limits the accretion of all other species. As a result, the abundances of species such as CO and  $NH_3$  show a near-steady state at a low coverage during this time. However, in the warm-up model, the increasing temperature increases the mobility of atomic hydrogen, which, in turn, produces molecular hydrogen, which can immediately desorb back to the gas phase freeing up the grain surface. The increase in temperature will also lead to an increase in the thermal desorption rate of atomic hydrogen. Thus, when the abundance of atomic hydrogen starts to decrease, the abundances and therefore the coverages of other species start to increase. A similar behavior can also be seen when chemisorbed CO attains a maximum coverage, resulting in the steplike abundance profile of  $NH_2$  and  $NH_3$ . The abundances of  $NH_2$  and  $NH_3$  only start to increase when



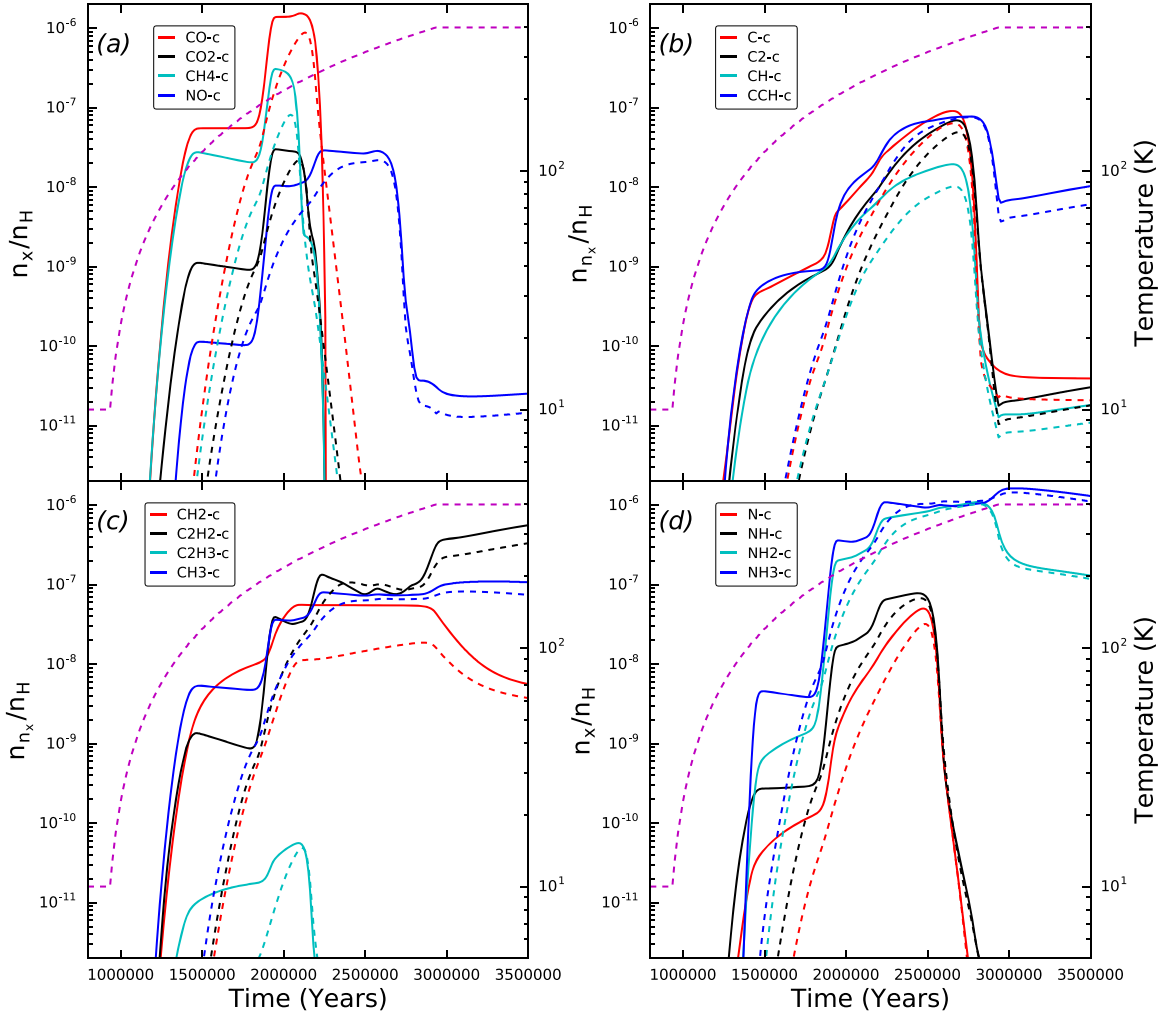


**Figure 9.** Fractional abundance of assorted chemisorbed molecules for the warm-up case. Solid and dashed lines represent models with an adsorption barrier of 0.1 eV and 0.2 eV, respectively. For both models, the temperature is increased from 10 to 400 K in  $2 \times 10^6$  yr, as shown by the dashed purple curve.

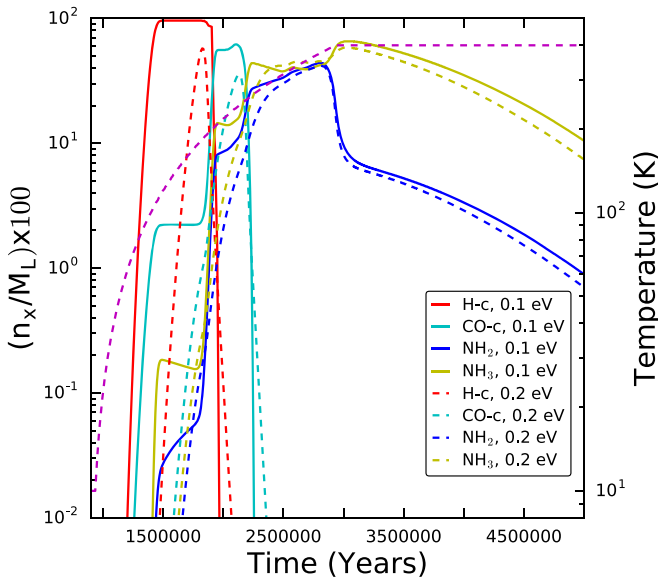


**Figure 10.** Percentage coverage of assorted molecules for the warm-up models with  $n_x$  the concentration of X in monolayers. Solid and dashed lines represent models with an adsorption barrier of 0.1 eV and 0.2 eV, respectively. For both models, temperature is increased from 10 to 400 K in  $2 \times 10^6$  yr.

chemisorbed CO starts to decrease. A similar behavior can be seen in the abundance profile of the other species. However, when the adsorption barrier is 0.2 eV, which makes accretion less efficient, we do not see any steplike structure in the coverage profiles, as is evident from Figure 10 (dashed lines).

It is obvious that the species having the lowest desorption energy for chemisorption crowds the grain provided it has a reasonably large gas-phase abundance. Then, unless it desorbs back to the gas phase or reacts to form a less volatile species, the grain is unavailable for adsorption of the other species, which is purely due to the assumption of one monolayer. This behavior can also be seen for physisorption at very low temperature ( $\leq 6$  K), when the grain can be full of immobile atoms (Katz et al. 1999). A corollary of this behavior is that in case the accretion is very efficient, the dust grain could have a large abundance ( $\sim 10^{-6}$ ) of a particular species depending upon its desorption energy. For most species, this effect can lead to a change in the gas abundance phase profile.

## 6. Conclusions

We have studied the chemistry of simple molecules on interstellar dust grains bound strongly by chemisorption on

**Table 8**  
Surface Reactions and Reactive Desorption

No.	Reaction	$E_a$ (K)	Fraction	Type <sup>a</sup>
Surface reactions				
1	c-C + c-C → c-C2	1.040E+04	9.000E-01	50
2	c-C + c-CH → c-CCH	1.040E+04	9.000E-01	50
3	c-C + c-CH2 → c-C2H2	1.102E+04	9.000E-01	50
4	c-C + c-CH3 → c-C2H3	1.110E+04	9.981E-01	50
5	c-C + c-O → c-CO	1.212E+04	9.000E-01	50
6	c-C + c-O2 → c-CO + c-O	1.306E+03	9.000E-01	50
7	c-CO + c-O → c-C + c-O2	9.134E+04	1.000E+00	50
8	c-C + c-OH → c-CO + c-H	4.701E+03	9.000E-01	50
9	c-CO + c-H → c-C + c-OH	8.024E+04	1.000E+00	50
10	c-CH + c-CH → c-C2H2	1.040E+04	9.000E-01	50
11	c-CH + c-CH2 → c-C2H3	1.102E+04	9.866E-01	50
12	c-CH + c-CH3 → c-C2H4	1.110E+04	9.970E-01	50
13	c-CH + c-O2 → c-HCO + c-O	1.306E+03	9.998E-01	50
14	c-HCO + c-O → c-CH + c-O2	5.828E+04	1.000E+00	50
15	c-CH2 + c-CH2 → c-C2H4	1.172E+04	9.960E-01	50
16	c-CH4 + c-CCH → c-C2H2 + c-CH3	8.237E+03	1.000E+00	50
17	c-C2H2 + c-CH3 → c-CH4 + c-CCH	2.316E+04	1.000E+00	50
18	c-H + c-C → c-CH	7.130E+03	9.000E-01	50
19	c-H + c-C2 → c-CCH	7.130E+03	9.000E-01	50
20	c-H + c-CCH → c-C2H2	7.284E+03	9.845E-01	50
21	c-H + c-C2H2 → c-C2H3	7.358E+03	1.000E+00	50
22	c-H + c-C2H3 → c-C2H4	7.394E+03	9.999E-01	50
23	c-H + c-CH → c-CH2	7.130E+03	9.195E-01	50
24	c-H + c-CH2 → c-CH3	7.417E+03	9.894E-01	50
25	c-H + c-CH3 → c-CH4	7.451E+03	9.931E-01	50
26	c-H + c-CH4 → c-CH3 + c-H2	5.936E+03	1.000E+00	50
27	c-H2 + c-CH3 → c-CH4 + c-H	1.881E+04	1.000E+00	50
28	c-H + c-CO → c-HCO	6.131E+03	1.000E+00	50
29	c-H + c-O → c-OH	7.899E+03	9.000E-01	50
30	c-H + c-OH → c-H2O	3.894E+03	9.000E-01	50
31	c-H2 + c-C → c-CH2	8.129E+03	9.951E-01	50
32	c-H2 + c-C2 → c-CCH + c-H	8.129E+03	1.000E+00	50
33	c-CCH + c-H → c-C2 + c-H2	2.406E+04	1.000E+00	50
34	c-H2 + c-CCH → c-C2H2 + c-H	8.330E+03	1.000E+00	50
35	c-H + c-C2H2 → c-CCH + c-H2	1.038E+04	1.000E+00	50
36	c-H2 + c-CH2 → c-CH3 + c-H	8.504E+03	1.000E+00	50
37	c-H + c-CH3 → c-CH2 + c-H2	9.574E+03	1.000E+00	50
38	c-H2 + c-OH → c-H2O + c-H	4.174E+03	1.000E+00	50
39	c-H + c-H2O → c-H2 + c-OH	8.814E+03	1.000E+00	50
40	c-O + c-CH → c-HCO	1.212E+04	9.000E-01	50
41	c-O + c-CO → c-CO2	9.492E+03	9.000E-01	50
42	c-O + c-HCO → c-CO2 + c-H	9.492E+03	9.984E-01	50
43	c-H + c-CO2 → c-HCO + c-O	4.674E+04	1.000E+00	50
44	c-O + c-HCO → c-CO + c-OH	9.492E+03	1.000E+00	50
45	c-OH + c-CO → c-HCO + c-O	3.005E+04	1.000E+00	50
46	c-O + c-O → c-O2	1.452E+04	9.000E-01	50
47	c-OH + c-CO → c-CO2 + c-H	4.245E+03	1.000E+00	50
48	c-H + c-CO2 → c-CO + c-OH	2.094E+04	1.000E+00	50
49	c-H + c-H → c-H2	5.425E+03	9.000E-01	50
50	c-N + c-H → c-NH	6.817E+03	9.000E-01	50
51	c-NH + c-H → c-NH2	6.817E+03	9.127E-01	50
52	c-NH2 + c-H → c-NH3	7.338E+03	9.890E-01	50
53	c-N + c-O → c-NO	1.124E+04	9.000E-01	50
54	c-N + c-C → c-CN	9.747E+03	9.000E-01	50
55	c-CN + c-H → c-HCN	7.131E+03	9.000E-01	50
Reactive Desorption				
56	c-C + c-C → C2	1.040E+04	1.000E-01	51
57	c-C + c-CH → CCH	1.040E+04	1.000E-01	51
58	c-C + c-CH2 → C2H2	1.102E+04	1.000E-01	51
59	c-C + c-CH3 → C2H3	1.110E+04	1.859E-03	51
60	c-C + c-O → CO	1.212E+04	1.000E-01	51
61	c-C + c-O2 → CO + O	1.306E+03	1.000E-01	51

**Table 8**  
(Continued)

No.	Reaction	$E_a$ (K)	Fraction	Type <sup>a</sup>
62	c-CO + c-O → C + O <sub>2</sub>	9.134E+04	0.000E+00	51
63	c-C + c-OH → CO + H	4.701E+03	1.000E-01	51
64	c-CO + c-H → C + OH	8.024E+04	0.000E+00	51
65	c-CH + c-CH → C <sub>2</sub> H <sub>2</sub>	1.040E+04	1.000E-01	51
66	c-CH + c-CH <sub>2</sub> → C <sub>2</sub> H <sub>3</sub>	1.102E+04	1.344E-02	51
67	c-CH + c-CH <sub>3</sub> → C <sub>2</sub> H <sub>4</sub>	1.110E+04	2.957E-03	51
68	c-CH + c-O <sub>2</sub> → HCO + O	1.306E+03	2.045E-04	51
69	c-HCO + c-O → CH + O <sub>2</sub>	5.828E+04	0.000E+00	51
70	c-CH <sub>2</sub> + c-CH <sub>2</sub> → C <sub>2</sub> H <sub>4</sub>	1.172E+04	4.019E-03	51
71	c-CH <sub>4</sub> + c-CCH → C <sub>2</sub> H <sub>2</sub> + CH <sub>3</sub>	8.237E+03	3.589E-35	51
72	c-C <sub>2</sub> H <sub>2</sub> + c-CH <sub>3</sub> → CH <sub>4</sub> + CCH	2.316E+04	0.000E+00	51
73	c-H + c-C → CH	7.130E+03	1.000E-01	51
74	c-H + c-C <sub>2</sub> → CCH	7.130E+03	1.000E-01	51
75	c-H + c-CCH → C <sub>2</sub> H <sub>2</sub>	7.284E+03	1.554E-02	51
76	c-H + c-C <sub>2</sub> H <sub>2</sub> → C <sub>2</sub> H <sub>3</sub>	7.358E+03	3.620E-18	51
77	c-H + c-C <sub>2</sub> H <sub>3</sub> → C <sub>2</sub> H <sub>4</sub>	7.394E+03	1.323E-04	51
78	c-H + c-CH → CH <sub>2</sub>	7.130E+03	8.052E-02	51
79	c-H + c-CH <sub>2</sub> → CH <sub>3</sub>	7.417E+03	1.055E-02	51
80	c-H + c-CH <sub>3</sub> → CH <sub>4</sub>	7.451E+03	6.872E-03	51
81	c-H + c-CH <sub>4</sub> → CH <sub>3</sub> + H <sub>2</sub>	5.936E+03	4.526E-27	51
82	c-H <sub>2</sub> + c-CH <sub>3</sub> → CH <sub>4</sub> + H	1.881E+04	0.000E+00	51
83	c-H + c-CO → HCO	6.131E+03	0.000E+00	51
84	c-H + c-O → OH	7.899E+03	1.000E-01	51
85	c-H + c-OH → H <sub>2</sub> O	3.894E+03	1.000E-01	51
86	c-H <sub>2</sub> + c-C → CH <sub>2</sub>	8.129E+03	4.947E-03	51
87	c-H <sub>2</sub> + c-C <sub>2</sub> → CCH + H	8.129E+03	2.820E-19	51
88	c-CCH + c-H → C <sub>2</sub> + H <sub>2</sub>	2.406E+04	0.000E+00	51
89	c-H <sub>2</sub> + c-CCH → C <sub>2</sub> H <sub>2</sub> + H	8.330E+03	4.265E-35	51
90	c-H + c-C <sub>2</sub> H <sub>2</sub> → CCH + H <sub>2</sub>	1.038E+04	0.000E+00	51
91	c-H <sub>2</sub> + c-CH <sub>2</sub> → CH <sub>3</sub> + H	8.504E+03	3.572E-37	51
92	c-H + c-CH <sub>3</sub> → CH <sub>2</sub> + H <sub>2</sub>	9.574E+03	0.000E+00	51
93	c-H <sub>2</sub> + c-OH → H <sub>2</sub> O + H	4.174E+03	1.172E-13	51
94	c-H + c-H <sub>2</sub> O → H <sub>2</sub> + OH	8.814E+03	0.000E+00	51
95	c-O + c-CH → HCO	1.212E+04	1.000E-01	51
96	c-O + c-CO → CO <sub>2</sub>	9.492E+03	1.000E-01	51
97	c-O + c-HCO → CO <sub>2</sub> + H	9.492E+03	1.649E-03	51
98	c-H + c-CO <sub>2</sub> → HCO + O	4.674E+04	0.000E+00	51
99	c-O + c-HCO → CO + OH	9.492E+03	4.120E-11	51
100	c-OH + c-CO → HCO + O	3.005E+04	0.000E+00	51
101	c-O + c-O → O <sub>2</sub>	1.452E+04	1.000E-01	51
102	c-OH + c-CO → CO <sub>2</sub> + H	4.245E+03	3.851E-09	51
103	c-H + c-CO <sub>2</sub> → CO + OH	2.094E+04	0.000E+00	51
104	c-H + c-H → H <sub>2</sub>	5.425E+03	1.000E-01	51
105	c-N + c-H → NH	6.817E+03	1.000E-01	51
106	c-NH + c-H → NH <sub>2</sub>	6.817E+03	8.731E-02	51
107	c-NH <sub>2</sub> + c-H → NH <sub>3</sub>	7.338E+03	1.098E-02	51
108	c-N + c-O → NO	1.124E+04	1.000E-01	51
109	c-N + c-C → c-CN	9.747E+03	1.000E-01	51
110	c-CN + c-H → c-HCN	7.132E+03	1.000E-01	51

**Note.**

<sup>a</sup> A number is assigned to show a type of reaction in our network. The “fraction” denotes the amount that stays (for type 50) on the surface or desorbs (type 51) to the gas phase due to reactive desorption.

graphite. Chemical simulations involving chemisorbed and gas-phase species have been run for both isothermal and warm-up conditions using simplified assumptions. The isothermal models were run between 150 and 400 K at an interval of 25 K, and the warm-up models have a temperature range between 10 and 400 K. For each case, we have run models with different values of adsorption barriers and binding energies to explore the sensitivity of our results to these uncertain chemisorption parameters. Our major conclusions are as follows.

1. The efficiency of chemisorption hinges strongly on the efficiency of adsorption. Models having the lowest adsorption barrier for all species (0.1 eV) were found to produce reasonably abundant chemisorbed species, although the abundance of a chemisorbed species depends both on the adsorption rate and also other processes such as its chemistry. The reduction by a factor of 2 of individual desorption energies calculated by us does not increase the abundances markedly.

**Table 9**  
Other Processes Involving Chemisorption

No.	Reaction	$E_a(K)$	Type <sup>a</sup>
Thermal desorption and photodesorption (53, 54) (No $E_A$ )			
111	c-C $\rightarrow$ C	...	52
112	c-C2 $\rightarrow$ C2	...	52
113	c-CCH $\rightarrow$ CCH	...	52
114	c-C2H2 $\rightarrow$ C2H2	...	52
115	c-C2H3 $\rightarrow$ C2H3	...	52
116	c-C2H4 $\rightarrow$ C2H4	...	52
117	c-C2H5 $\rightarrow$ C2H5	...	52
118	c-CH $\rightarrow$ CH	...	52
119	c-CH2 $\rightarrow$ CH2	...	52
120	c-CH3 $\rightarrow$ CH3	...	52
121	c-CH4 $\rightarrow$ CH4	...	52
122	c-CO $\rightarrow$ CO	...	52
123	c-CO2 $\rightarrow$ CO2	...	52
124	c-H $\rightarrow$ H	...	52
125	c-H2 $\rightarrow$ H2	...	52
126	c-H2O $\rightarrow$ H2O	...	52
127	c-HCO $\rightarrow$ HCO	...	52
128	c-O $\rightarrow$ O	...	52
129	c-O2 $\rightarrow$ O2	...	52
130	c-OH $\rightarrow$ OH	...	52
131	c-N $\rightarrow$ N	...	52
132	c-NH $\rightarrow$ NH	...	52
133	c-NH2 $\rightarrow$ NH2	...	52
134	c-NH3 $\rightarrow$ NH3	...	52
135	c-NO $\rightarrow$ NO	...	52
136	c-CN $\rightarrow$ CN	...	52
137	c-HCN $\rightarrow$ HCN	...	52
Thermal dissociation			
		$E_a(K)$	Type <sup>a</sup>
192	c-C2 $\rightarrow$ c-C + c-C	6.078E+04	55
193	c-CCH $\rightarrow$ c-C2 + c-H	6.681E+04	55
194	c-C2H2 $\rightarrow$ c-CCH + c-H	5.309E+04	55
195	c-C2H3 $\rightarrow$ c-C2H2 + c-H	1.450E+04	55
196	c-C2H4 $\rightarrow$ c-C2H2 + c-H2	1.649E+04	55
197	c-CH $\rightarrow$ c-C + c-H	3.698E+04	55
198	c-CH3 $\rightarrow$ c-CH2 + c-H	5.223E+04	55
199	c-CH4 $\rightarrow$ c-CH2 + c-H2	4.045E+04	55
200	c-CO $\rightarrow$ c-C + c-O	1.050E+05	55
201	c-CO2 $\rightarrow$ c-CO + c-O	4.353E+04	55
202	c-H2O $\rightarrow$ c-OH + c-H	5.228E+04	55
203	c-HCO $\rightarrow$ c-CO + c-H	2.921E+03	55
204	c-O2 $\rightarrow$ c-O + c-O	1.737E+04	55
205	c-OH $\rightarrow$ c-O + c-H	2.524E+04	55
206	c-C2H2 $\rightarrow$ c-C2 + c-H + c-H	1.126E+05	55
207	c-C2H2 $\rightarrow$ c-CH + c-CH	1.066E+05	55
208	c-C2H4 $\rightarrow$ c-C2H2 + c-H + c-H	5.916E+04	55
209	c-C2H4 $\rightarrow$ c-C2H3 + c-H	5.206E+04	55
210	c-CH2 $\rightarrow$ c-C + c-H2	3.640E+04	55
211	c-CH2 $\rightarrow$ c-CH + c-H	4.930E+04	55
212	c-CH2 $\rightarrow$ c-C + c-H + c-H	7.914E+04	55
213	c-CH3 $\rightarrow$ c-C + c-H2 + c-H	8.121E+04	55
214	c-CH3 $\rightarrow$ c-CH + c-H + c-H	9.411E+04	55
215	c-CH3 $\rightarrow$ c-CH + c-H2	5.136E+04	55
216	c-CH4 $\rightarrow$ c-CH + c-H2 + c-H	8.224E+04	55
217	c-CH4 $\rightarrow$ c-CH3 + c-H	3.833E+04	55
218	c-CCH $\rightarrow$ c-CH + c-C	9.061E+04	55
219	c-C2H3 $\rightarrow$ c-CCH + c-H2	1.753E+04	55
220	c-C2H3 $\rightarrow$ c-CCH + c-H + c-H	6.023E+04	55
221	c-H2O $\rightarrow$ c-H2 + c-O	3.113E+04	55
222	c-H2O $\rightarrow$ c-O + c-H + c-H	7.363E+04	55
223	c-H2 $\rightarrow$ c-H + c-H	5.460E+04	55
224	c-CO2 $\rightarrow$ c-O + c-CO	4.813E+04	55

**Table 9**  
(Continued)

No.	Reaction	$E_a(K)$	Type <sup>a</sup>
225	c-NH $\rightarrow$ c-N + c-H	3.350E+04	55
226	c-NH2 $\rightarrow$ c-NH + c-H	4.860E+04	55
227	c-NH3 $\rightarrow$ c-NH2 + c-H	5.132E+04	55
228	c-NO $\rightarrow$ c-N + c-O	5.926E+04	55
229	c-CN $\rightarrow$ c-N + c-C	8.154E+04	55
230	c-HCN $\rightarrow$ c-CN + c-H	5.577E+04	55
Photodissociation processes of various types (No $E_A$ )			
231	c-C2 $\rightarrow$ c-C + c-C	...	56
232	c-C2 $\rightarrow$ c-C + c-C	...	60
233	c-C2 $\rightarrow$ c-C + c-C	...	61
234	c-CCH $\rightarrow$ c-C2 + c-H	...	56
235	c-CCH $\rightarrow$ c-C2 + c-H	...	60
236	c-CCH $\rightarrow$ c-C2 + c-H	...	61
237	c-C2H2 $\rightarrow$ c-CCH + c-H	...	56
238	c-C2H2 $\rightarrow$ c-CCH + c-H	...	57
239	c-C2H2 $\rightarrow$ c-CCH + c-H	...	60
240	c-C2H2 $\rightarrow$ c-CCH + c-H	...	61
241	c-C2H3 $\rightarrow$ c-C2H2 + c-H	...	56
242	c-C2H3 $\rightarrow$ c-C2H2 + c-H	...	60
243	c-C2H3 $\rightarrow$ c-C2H2 + c-H	...	61
244	c-C2H4 $\rightarrow$ c-C2H2 + c-H2	...	56
245	c-C2H4 $\rightarrow$ c-C2H2 + c-H2	...	57
246	c-C2H4 $\rightarrow$ c-C2H2 + c-H2	...	60
247	c-C2H4 $\rightarrow$ c-C2H2 + c-H2	...	61
248	c-CH $\rightarrow$ c-C + c-H	...	56
249	c-CH $\rightarrow$ c-C + c-H	...	60
250	c-CH $\rightarrow$ c-C + c-H	...	61
251	c-CH3 $\rightarrow$ c-CH2 + c-H	...	56
252	c-CH3 $\rightarrow$ c-CH2 + c-H	...	57
253	c-CH3 $\rightarrow$ c-CH2 + c-H	...	60
254	c-CH3 $\rightarrow$ c-CH2 + c-H	...	61
255	c-CH4 $\rightarrow$ c-CH2 + c-H2	...	56
256	c-CH4 $\rightarrow$ c-CH2 + c-H2	...	60
257	c-CO $\rightarrow$ c-C + c-O	...	56
258	c-CO $\rightarrow$ c-C + c-O	...	60
259	c-CO2 $\rightarrow$ c-CO + c-O	...	56
260	c-CO2 $\rightarrow$ c-CO + c-O	...	60
261	c-H2O $\rightarrow$ c-OH + c-H	...	56
262	c-H2O $\rightarrow$ c-OH + c-H	...	60
263	c-H2O $\rightarrow$ c-OH + c-H	...	61
264	c-HCO $\rightarrow$ c-CO + c-H	...	56
265	c-HCO $\rightarrow$ c-CO + c-H	...	57
266	c-HCO $\rightarrow$ c-CO + c-H	...	61
267	c-O2 $\rightarrow$ c-O + c-O	...	56
268	c-O2 $\rightarrow$ c-O + c-O	...	57
269	c-O2 $\rightarrow$ c-O + c-O	...	60
270	c-O2 $\rightarrow$ c-O + c-O	...	61
271	c-OH $\rightarrow$ c-O + c-H	...	56
272	c-OH $\rightarrow$ c-O + c-H	...	60
273	c-OH $\rightarrow$ c-O + c-H	...	61
274	c-C2H2 $\rightarrow$ c-C2 + c-H + c-H	...	57
275	c-C2H2 $\rightarrow$ c-C2 + c-H + c-H	...	61
276	c-C2H2 $\rightarrow$ c-CH + c-CH	...	57
277	c-C2H2 $\rightarrow$ c-CH + c-CH	...	61
278	c-C2H4 $\rightarrow$ c-C2H2 + c-H + c-H	...	57
279	c-C2H4 $\rightarrow$ c-C2H2 + c-H + c-H	...	61
280	c-C2H4 $\rightarrow$ c-C2H3 + c-H	...	57
281	c-C2H4 $\rightarrow$ c-C2H3 + c-H	...	61
282	c-CH2 $\rightarrow$ c-C + c-H2	...	57
283	c-CH2 $\rightarrow$ c-C + c-H2	...	61
284	c-CH2 $\rightarrow$ c-CH + c-H	...	56
285	c-CH2 $\rightarrow$ c-CH + c-H	...	57



**Table 9**  
(Continued)

No.	Reaction	$E_a$ (K)	Type <sup>a</sup>
286	c-CH <sub>2</sub> → c-CH + c-H	...	60
287	c-CH <sub>2</sub> → c-CH + c-H	...	61
288	c-CH <sub>2</sub> → c-C + c-H + c-H	...	57
289	c-CH <sub>2</sub> → c-C + c-H + c-H	...	61
290	c-CH <sub>3</sub> → c-C + c-H <sub>2</sub> + c-H	...	57
291	c-CH <sub>3</sub> → c-C + c-H <sub>2</sub> + c-H	...	61
292	c-CH <sub>3</sub> → c-CH + c-H + c-H	...	57
293	c-CH <sub>3</sub> → c-CH + c-H + c-H	...	61
294	c-CH <sub>3</sub> → c-CH + c-H <sub>2</sub>	...	57
295	c-CH <sub>3</sub> → c-CH + c-H <sub>2</sub>	...	60
296	c-CH <sub>3</sub> → c-CH + c-H <sub>2</sub>	...	61
297	c-CH <sub>4</sub> → c-CH + c-H <sub>2</sub> + c-H	...	60
298	c-CH <sub>4</sub> → c-CH <sub>3</sub> + c-H	...	60
299	c-CCH → c-CH + c-C	...	61
300	c-C <sub>2</sub> H <sub>3</sub> → c-CCH + c-H <sub>2</sub>	...	61
301	c-C <sub>2</sub> H <sub>3</sub> → c-CCH + c-H + c-H	...	61
302	c-H <sub>2</sub> O → c-H <sub>2</sub> + c-O	...	61
303	c-H <sub>2</sub> O → c-O + c-H + c-H	...	61
304	c-NH → c-N + c-H	...	56
305	c-NH → c-N + c-H	...	61
306	c-NH <sub>2</sub> → c-NH + c-H	...	56
307	c-NH <sub>2</sub> → c-NH + c-H	...	57
308	c-NH <sub>2</sub> → c-NH + c-H	...	60
309	c-NH <sub>2</sub> → c-NH + c-H	...	61
310	c-NH <sub>3</sub> → c-NH <sub>2</sub> + c-H	...	56
311	c-NH <sub>3</sub> → c-NH <sub>2</sub> + c-H	...	57
312	c-NH <sub>3</sub> → c-NH <sub>2</sub> + c-H	...	60
313	c-NH <sub>3</sub> → c-NH <sub>2</sub> + c-H	...	61
314	c-NO → c-N + c-O	...	56
315	c-NO → c-N + c-O	...	57
316	c-NO → c-N + c-O	...	60
317	c-NO → c-N + c-O	...	61
318	c-H <sub>2</sub> → c-H + c-H	...	56
319	c-H <sub>2</sub> → c-H + c-H	...	60
320	c-HCN → c-CN + c-H	...	56
321	c-HCN → c-CN + c-H	...	60
322	c-CN → c-C + c-N	...	56
323	c-CN → c-C + c-N	...	60
Eley–Rideal Reactions		$E_a$ (K)	Type <sup>a</sup>
324	C + c-H <sub>2</sub> → c-CH <sub>2</sub>	2.300E+03	58
325	C + c-C → c-C <sub>2</sub>	2.300E+03	58
326	C + c-CH → c-CCH	2.300E+03	58
327	CH + c-C → c-CCH	2.300E+03	58
328	C + c-CH <sub>2</sub> → c-C <sub>2</sub> H <sub>2</sub>	2.300E+03	58
329	CH <sub>2</sub> + c-C → c-C <sub>2</sub> H <sub>2</sub>	2.300E+03	58
330	C + c-CH <sub>3</sub> → c-C <sub>2</sub> H <sub>3</sub>	2.300E+03	58
331	CH <sub>3</sub> + c-C → c-C <sub>2</sub> H <sub>3</sub>	2.300E+03	58
332	C + c-O → c-CO	2.300E+03	58
333	O + c-C → c-CO	2.300E+03	58
334	C + c-O <sub>2</sub> → c-CO <sub>2</sub>	2.300E+03	58
335	O <sub>2</sub> + c-C → c-CO <sub>2</sub>	2.300E+03	58
336	CH + c-CH → c-C <sub>2</sub> H <sub>2</sub>	0	58
337	CH + c-CH <sub>2</sub> → c-C <sub>2</sub> H <sub>3</sub>	0	58
338	CH <sub>2</sub> + c-CH → c-C <sub>2</sub> H <sub>3</sub>	0	58
339	CH <sub>3</sub> + c-CH → c-C <sub>2</sub> H <sub>4</sub>	0	58
340	CH + c-CH <sub>3</sub> → c-C <sub>2</sub> H <sub>4</sub>	0	58
341	CH <sub>2</sub> + c-CH <sub>2</sub> → c-C <sub>2</sub> H <sub>4</sub>	0	58
342	H + c-C → c-CH	0	58
343	C + c-H → c-CH	0	58
344	H + c-C <sub>2</sub> → c-CCH	0	58
345	C <sub>2</sub> + c-H → c-CCH	0	58
346	H + c-CCH → c-C <sub>2</sub> H <sub>2</sub>	0	58
347	CCH + c-H → c-C <sub>2</sub> H <sub>2</sub>	0	58

**Table 9**  
(Continued)

No.	Reaction	$E_a$ (K)	Type <sup>a</sup>
348	H + c-C <sub>2</sub> H <sub>2</sub> → c-C <sub>2</sub> H <sub>3</sub>	0	58
349	C <sub>2</sub> H <sub>2</sub> + c-H → c-C <sub>2</sub> H <sub>3</sub>	0	58
350	H + c-C <sub>2</sub> H <sub>3</sub> → c-C <sub>2</sub> H <sub>4</sub>	0	58
351	C <sub>2</sub> H <sub>3</sub> + c-H → c-C <sub>2</sub> H <sub>4</sub>	0	58
352	H + c-CH → c-CH <sub>2</sub>	0	58
353	CH + c-H → c-CH <sub>2</sub>	0	58
354	H + c-CH <sub>2</sub> → c-CH <sub>3</sub>	0	58
355	CH <sub>2</sub> + c-H → c-CH <sub>3</sub>	0	58
356	H + c-CH <sub>3</sub> → c-CH <sub>4</sub>	0	58
357	CH <sub>3</sub> + c-H → c-CH <sub>4</sub>	0	58
358	H + c-CO → c-HCO	0	58
359	CO + c-H → c-HCO	0	58
360	H + c-O → c-OH	0	58
361	O + c-H → c-OH	0	58
362	H + c-OH → c-H <sub>2</sub> O	0	58
363	OH + c-H → c-H <sub>2</sub> O	0	58
364	N + c-H → c-NH	0	58
365	H + c-N → c-NH	0	58
366	H + c-NH → c-NH <sub>2</sub>	0	58
367	NH + c-H → c-NH <sub>2</sub>	0	58
368	NH <sub>2</sub> + c-H → c-NH <sub>3</sub>	0	58
369	H + c-NH <sub>2</sub> → c-NH <sub>3</sub>	0	58
370	O + c-N → c-NO	2.300E+03	58
371	N + c-O → c-NO	2.300E+03	58
372	C + c-N → c-CN	2.300E+03	58
373	N + c-C → c-CN	2.300E+03	58
374	H + c-CN → c-HCN	0	58
Accretion <sup>b</sup>		$E_a$ (K)	Type <sup>a</sup>
375	C → c-C	...	59
376	C <sub>2</sub> → c-C <sub>2</sub>	...	59
377	CCH → c-CCH	...	59
378	C <sub>2</sub> H <sub>2</sub> → c-C <sub>2</sub> H <sub>2</sub>	...	59
379	C <sub>2</sub> H <sub>3</sub> → c-C <sub>2</sub> H <sub>3</sub>	...	59
380	C <sub>2</sub> H <sub>4</sub> → c-C <sub>2</sub> H <sub>4</sub>	...	59
381	C <sub>2</sub> H <sub>5</sub> → c-C <sub>2</sub> H <sub>5</sub>	...	59
382	CH → c-CH	...	59
383	CH <sub>2</sub> → c-CH <sub>2</sub>	...	59
384	CH <sub>3</sub> → c-CH <sub>3</sub>	...	59
385	CH <sub>4</sub> → c-CH <sub>4</sub>	...	59
386	CO → c-CO	...	59
387	CO <sub>2</sub> → c-CO <sub>2</sub>	...	59
388	H → c-H	...	59
389	H <sub>2</sub> → c-H <sub>2</sub>	...	59
390	H <sub>2</sub> O → c-H <sub>2</sub> O	...	59
391	HCO → c-HCO	...	59
392	O → c-O	...	59
393	O <sub>2</sub> → c-O <sub>2</sub>	...	59
394	OH → c-OH	...	59
395	N → c-N	...	59
396	NH → c-NH	...	59
397	NH <sub>2</sub> → c-NH <sub>2</sub>	...	59
398	NH <sub>3</sub> → c-NH <sub>3</sub>	...	59
399	NO → c-NO	...	59
401	CN → c-CN	...	59
402	HCN → c-HCN	...	59

**Notes.**<sup>a</sup> A number is assigned to show a type of reaction in our network.<sup>b</sup> Models with three different adsorption barriers (0.1, 0.2, and 0.3 eV) are run as discussed in the text.

2. For species such as CO, which are very efficiently formed in the gas phase at almost all temperatures (10–400 K), the existence of chemisorbed molecules will not have a significant impact on their gas-phase abundances. However, some chemisorbed CO can be locked on grains, leading to a reasonably high abundance of  $\sim 10^{-6}$ , so that it could be detectable using upcoming observational facilities. Species such as  $C_2H_2$  and  $NH_3$ , which are less efficiently formed in the gas phase compared with CO, may show a change in their gas-phase abundances due to chemisorption. The chemisorbed species can also approach peak abundances near  $\sim 10^{-6}$  and may be detectable.
3. A reasonably large number of chemisorbed species show fractional abundances above  $10^{-8}$  under certain conditions. An attempt to detect them using *JWST* might be worthwhile if chemisorbed species with higher abundances can be detected with reasonable signal to noise.
4. For warm-up models, if the efficiency of adsorption is high, a step-like abundance profile versus time is calculated using the assumption that chemisorption is possible only in the first monolayer, which rules out the formation of more than one layer.
5. Our calculations are based on the scant existing literature and simplified assumptions. In the future, detailed quantum mechanical calculations and experiments will be required to extract essential parameters such as diffusion barriers, sticking coefficients, adsorption barriers, and activation energies for many reactions on astrophysically relevant surfaces in order to understand better the potential of chemisorption for astrophysical systems.
6. Finally, we restricted our calculations to so-called classical grains of  $10^{-5}$  cm radius; however, in reality, grains are distributed in size. Because smaller grains are much larger in number, they will likely contribute more toward the overall abundance of chemisorbed species. A more detailed study involving a granular size distribution may be done in the future. Similarly, an extension of our work to a variety of sources, especially AGB stars, as suggested by the referee, may also be accomplished.

We acknowledge the excellent report of the referee, who brought up important points such as the role of grain size distributions and the likelihood of which types of sources might be best for detecting chemisorbed species. The support of the National Science Foundation (US) for the astrochemistry program of E. H. (grant No. AST-1906489) is kindly acknowledged. The results presented here are based on computations using the 3TFLOP HPC Cluster at the Physical Research Laboratory, Ahmedabad, India.

### Appendix Tabulation of Processes

In this appendix, we present two tables (Tables 8 and 9) containing all of the reactions and processes associated with chemisorption in our expanded gas–grain network. Chemisorbed species are designated with a c-. The processes are divided into types of chemical and physical processes involved with chemisorption in our expanded network; each process is given a number standing for the type of process in the code utilized. The processes are also included in Figure 1. The order

here is as follows: surface diffusive reactions (type 50), reactive desorption (type 51), thermal desorption (type 52), photo-desorption via external radiation (53), photodesorption via cosmic-ray production of internal photons (54), thermal dissociation (55), photodissociation via cosmic-ray production of internal photons (56, 57) and via external photons (60, 61), ER reactions (58), and accretion (adsorption) (59). Photo-dissociation types 57 and 61 refer to unusual processes in which the initial step is a surface photoionization followed immediately by dissociative recombination to form the same surface neutral species as the regular processes. For each process, an activation energy barrier ( $E_a$  (K)) is included if nonzero, the value of which depends upon the process and the individual reaction. Fixed barriers for each reaction in a process are not included. These include an adsorption barrier of 0.1 eV, 0.2 eV, or 0.3 eV, only one of which is used for all adsorption (accretion) processes in a given calculation, and a diffusive barrier defined by 0.5 of the desorption energy. Values of the desorption energy, important for thermal desorption, can be found in Table 1 but are not strictly barriers.

For exothermic surface reactions, the chemical activation energy is defined by Equations (8)–(9), depending upon which is larger. The expression  $D_{AB}$  in these formulae is the exothermicity of the reaction in the gas phase. In the one or two cases which are endothermic, we used Equation (10) to determine the activation energy. For reactive desorption, the same approach is used as for exothermic surface reactions, but the fraction that is desorbed must be calculated separately. For thermal dissociation, these endothermic processes will have activation barriers given by Equation (10). Finally, for ER processes, we have followed the assumption discussed in the body of the text, in which collisions involving the gas-phase species and the adsorbate have a barrier of 0.2 eV unless reactive species such as atomic hydrogen are involved.

### ORCID iDs

Kinsuk Acharyya  <https://orcid.org/0000-0002-0603-8777>

Eric Herbst  <https://orcid.org/0000-0002-4649-2536>

### References

- Acharyya, K., & Herbst, E. 2017, *ApJ*, **850**, 105  
 Allen, M., & Robinson, G. W. 1977, *ApJ*, **212**, 396  
 Allouche, A., Ferro, Y., Angot, T., Thomas, C., & Layet, J.-M. 2005, *JChPh*, **123**, 124701  
 Arfou, E., Cartry, G., Layet, J.-M., & Angot, T. 2011, *JChPh*, **134**, 014701  
 Boyd, D. A., Hess, F. M., & Hess, G. B. 2002, *SurSc*, **519**, 125  
 Brown, P. D., Charnley, S. B., & Millar, T. J. 1988, *MNRAS*, **231**, 409  
 Cazaux, S., & Tielens, A. G. G. M. 2002, *ApJ*, **575L**, 29C  
 Chakrapani, N., Zhang, Y. M., Nayak, S. K., et al. 2003, *JPCB*, **107**, 9308  
 Ferro, Y., Marinelli, F., & Allouche, A. 2002, *JChPh*, **116**, 8124  
 Ferro, Y., Marinelli, F., & Allouche, A. 2003, *CPL*, **368**, 609  
 Garrod, R. T., Wakelam, V., & Herbst, E. 2007, *A&A*, **467**, 1103  
 Garrod, R. T., Widicus-Weaver, S. L., & Herbst, E. 2008, *ApJ*, **682**, 283  
 Harada, N., Herbst, E., & Wakelam, V. 2010, *ApJ*, **721**, 1570  
 Hasegawa, T., & Herbst, E. 1993, *MNRAS*, **261**, 83  
 Hasegawa, T., Herbst, E., & Leung, C. M. 1992, *ApJS*, **82**, 167  
 Herbst, E. 2017, *IRPC*, **36**, 287  
 Herbst, E., & Klemperer, W. 1973, *ApJ*, **185**, 505  
 Herbst, E., & Millar, T. J. 2008, in *Low Temperatures and Cold Molecules*, ed. I. W. M. Smith (London: Imperial College Press), 1  
 Herbst, E., & van Dishoeck, E. F. 2009, *ARA&A*, **47**, 427  
 Incze, A., Pasturel, A., & Chatillon, C. 2001, *ApSS*, **177**, 226  
 Incze, A., Pasturel, A., & Chatillon, C. 2003, *SurSc*, **537**, 55  
 Iqbal, W., Acharyya, K., & Herbst, E. 2012, *ApJ*, **751**, 58  
 Iqbal, W., Acharyya, K., & Herbst, E. 2014, *ApJ*, **784**, 139

- Jelea, A., Marinelli, F., Ferro, Y., Allouche, A., & Brosset, C. 2004, *Carbon*, 42, 3189
- Karlický, F., Lepetit, B., & Lemoine, D. 2014, *JChPh*, 140, 124702
- Katz, N., Furman, I., Biham, O., Pirronello, V., & Vidali, G. , 1999, *ApJ*, 522, 305
- Kelemen, S. R., & Freund, H. 1985, *Carbon*, 6, 619
- Kerwin, J., & Jackson, B. 2008, *JChPh*, 128, 084702
- Klose, S. 1992, *A&A*, 260, 321
- Kolasinski, K. W. 2002, *Surface Science: Foundations of Catalysis and Nanoscience* (West Sussex: Wiley)
- Kress, M. E., & Tielens, A. G. G. M. 2001, *M&PS*, 36, 75
- Liu, F., Chu, W., Sun, W., Xue, Y., & Jiang, Q. 2012, *J. Nat. Gas Chem.*, 21, 708
- Mandeltort, L., Choudhury, P., Johnson, J. K., & Yates, J. T., Jr. 2012, *J. Phys. Chem. C*, 116, 18347
- Marchon, B., Tysoe, W. T., Carrazza, J., Heinemann, H., & Somorjait, G. A. 1988, *JPhCh*, 92, 5744
- Millar, T. J., & Freeman, A. 1984, *MNRAS*, 207, 405
- Moròn, V., Gamallo, P., & Sayós, R. 2010, *Theor. Chem. Accounts* 2010, 128, 683
- Öberg, K. I., Boogert, A. C. A., Pontoppidan, K. M., et al. 2008, *ApJ*, 678, 1032
- Öberg, K. I., Linnartz, H., Visser, R., & van Dishoeck, E. F. 2009a, *ApJ*, 693, 1209
- Öberg, K. I., van Dishoeck, E. F., & Linnartz, H. 2009b, *A&A*, 496, 281
- Pickles, J. B., & Williams, D. A. 1977, *ApSS*, 52, 453
- Pritchard, J., Catterick, T., & Gupta, R. K. 1975, *SurSc*, 53, 1
- Ruad, M., Loison, J. C., Hickson, K. M., et al. 2015, *MNRAS*, 447, 4004
- Sha, X., & Jackson, B. 2002, *SurSc*, 496, 318
- Sha, X., Jackson, B., Lemoine, D., & Lepetit, B. 2005, *JChPh*, 122, 014709
- Shustorovich, E. 1988, *Accounts Chem. Res.*, 21, 183
- Tait, S. L., Dohnalek, Z., Campbell, C. T., & Kay, B. D. 2006, *JChPh*, 125, 234308
- Tielens, A. G. G. M., & Hagen, W. 1982, *A&A*, 114, 245
- Wakelam, V., & Herbst, E. 2008, *ApJ*, 680, 371
- Wakelam, V., Loison, J.-C., Herbst, R. E., et al. 2014, *ApJS*, 217, 20
- Yates, J., Jr., Duncan, T. M., & Vaughan, R. W. 1979, *JChPh*, 71, 3908
- Zecho, T., Güttler, A., & Küppers, J. 2004, *Carbon*, 42, 609
- Zecho, T., Güttler, A., Sha, X., Jackson, B., & Küppers, J. 2002, *JChPh*, 117, 8486